INSTITUT FÜR ANGEWANDTE PHYSIK
GOETHE UNIVERSITÄT FRANKFURT

Beam Loss and Beam Shape at the LHC Collimators

Florian BURKART

Supervisors:
Prof. Dr. U. Ratzinger (IAP, Goethe Universität)
Dr. R. W. Aßmann (BE-ABP, CERN)

Goethe Universität Frankfurt/Main
Masterarbeit
Beam Loss and Beam Shape at the LHC Collimators

Florian Burkart

25th March 2012

CONTENTS

1. ABSTRACT

In this master thesis the beam loss and the beam shape at the LHC collimators was measured, analysed, presented and discussed.
Beginning with a short introduction of the LHC, the experiments, the superconducting magnet system, the basics on linear beam dynamics and a describtion of the LHC collimation system are given.
This is followed by the presentation of the performance of the LHC collimation system during 2011. A method to convert the Beam Loss Monitor signal in Gy/s to a proton beam loss rate will be introduced. Also the beam lifetime during the proton physics runs in 2011 will be presented and discussed. Finally, the shape of the LHC beams is analysed by using data obtained by scraping the beam at the LHC primary collimators.

2. KURZBESCHREIBUNG

Ziel dieser Master-Arbeit war es die Teilchenverluste und die transversale Teilchenverteilung der Protonenstrahlen an den Kollimatoren des Large Hadron Collider am CERN zu vermessen.
Zu Beginn der Arbeit wird eine kurze Einführung in den Aufbau und die Funktionsweise des zirkularen Beschleunigers LHC gegeben. Dem folgt eine Präsentation der Grundlagen der linearen Strahldynamik und des LHC Kollimationssystems.
Im zweiten Teil dieser Arbeit wird die Qualität des LHC Kollimationssystems während des Betriebes im Jahr 2011 vorgestellt und eine Methode beschrieben, welche es ermöglicht das Signal der Detektoren für Strahlverluste, welches in Gy/s gemessen wird, zu einer Teilchenverlustrate in p/s umzurechen.
Ein Kapitel ist der Lebensdauer der LHC Protonenstrahlen gewidmet sein. Die Analyse für das Jahr 2011 wird vorgestellt und diskutiert. Schlussendlich wird das sogenannte *Beam scraping* beschrieben, mit welchem es möglich war, die transversale Teilchenverteilung im LHC zu bestimmen.

3. INTRODUCTION

The Large Hadron Collider (LHC) at CERN was designed to accelerate and store particle beams of up to intensities of 3×10^{14} protons and a particle momentum of 7 TeV/c. This leads to a stored beam energy of 360 MJ, which is stored in the superconducting magnet system environment of the LHC. This beam energy would be enough to melt a block of 420 kg of Copper. The superconducting magnets would quench even if there is only a small fraction of particles which get lost.

The high intensity beams and beam momenta in the LHC make a sophisticated beam cleaning necessary. The LHC four-stage cleaning system was therefore designed to intercept and absorb unavoidable particle losses. 88 movable collimators were installed in the 27 km long ring of the LHC to guarantee safe physics operation. Within this master thesis the beam loss and the beam shape at the LHC primary collimators is described.

The master thesis will start with an overview of the LHC, the four main experiments installed in the ring, the superconducting magnet system and the collimation system. Also, the basics in linear beam dynamics and reasons for beam losses will be briefly introduced.
In the second part, the qualification of the LHC collimation system will be explained and a so-called loss map will be introduced. Also the performance and the achieved beam loss rate of the LHC collimation system in 2011 is presented.
For beam shape studies with the 110 MJ beams the so-called primary collimators were moved into the beams to scrape away the particles. This measurement procedure and the results of the first sets of full beam scrapings in the horizontal, vertical and skew planes will be presented and discussed.
At the end of this master thesis the analysis of the collimation dependent beam lifetime will be explained and the results for the proton physics fills in 2011 will be discussed. This analysis also gives an insight of the behaviour of the machine after changing settings like tune or β^*.
A summary of the results of LHC collimation system performance, beam shape and the instantaneous beam lifetimes is given in the conclusion.

4. THE LARGE HADRON COLLIDER

The **L**arge **H**adron **C**ollider (LHC) at the European Organization for Nuclear Research (CERN) in Geneva is the worlds biggest accelerator ever built. The LHC is a circular proton-proton, ion-proton or ion-ion collider which accelerates and stores beams up to a design particle momentum of 7 TeV/c. Lead ions were used for the ion operation. This high energy and the high collision rate will bring the knowledge of high energy particle physics to a new regime. Four major experiments located in the LHC search i.e. for new particles (like the Higgs Boson) or supersymmetry.

Within this chapter a short overview of the LHC is given. The four major experiments and the superconducting magnet system, which is necessary to keep the high intensity beams on their trajectory, will be briefly introduced. Then the two so-called cleaning insertions with collimators will be introduced. There will be an introduction of the linear beam dynamics in particle accelerators with the equation of motion and the longitudinal and transverse motion of charged particles in the second part of the chapter. Also the LHC aperture will be briefly explained.

This thesis will focus on protons, as measurements and calculations were done with these particles.

4.1 The Large Hadron Collider

The LHC is a circular particle accelerator with a circumference of 26.659 km in the underground (average 100 m depth) of the swiss-french border region near Geneva. It is located in the tunnel of the former **L**arge **E**lectron-**P**ositron Collider (LEP). Other, smaller particle accelerators, also called pre-injectors, are used to get the beams into the LHC. This injector chain begins with the **lin**ear **ac**celerator (LINAC 2), followed by the Booster, the **P**roton **S**ynchrotron (PS) and the **S**uper **P**roton **S**ynchrotron. An overview of the CERN accelerator complex is given in Figure 4.1.

The basic layout of the LHC [1, 2] is formed by eight arcs, hosting 23 so-called FODO cells, and eight straight sections, the so-called **I**nteraction **R**egions (IRs). In these IRs the four major experiments are located. The beams collide inside the experimental areas in the **I**nteraction **P**oints (IPs), where the experiments ATLAS (IP1), ALICE (IP2), CMS (IP5) and LHCb (IP8) are placed. The two counter rotating beams are injected in IR2 and IR8 respectively and accelerated by radio frequency cavities, positioned in IR4, up to a currently maximum allowed particle momentum of 3.5 TeV (2011) or 4 TeV (2012).

After the acceleration the beams are squeezed to reduce the beam size and then are brought into collision. Under normal conditions the beams are stored for up to 14 hours. At the end of physics operation or in case of failures the beams are

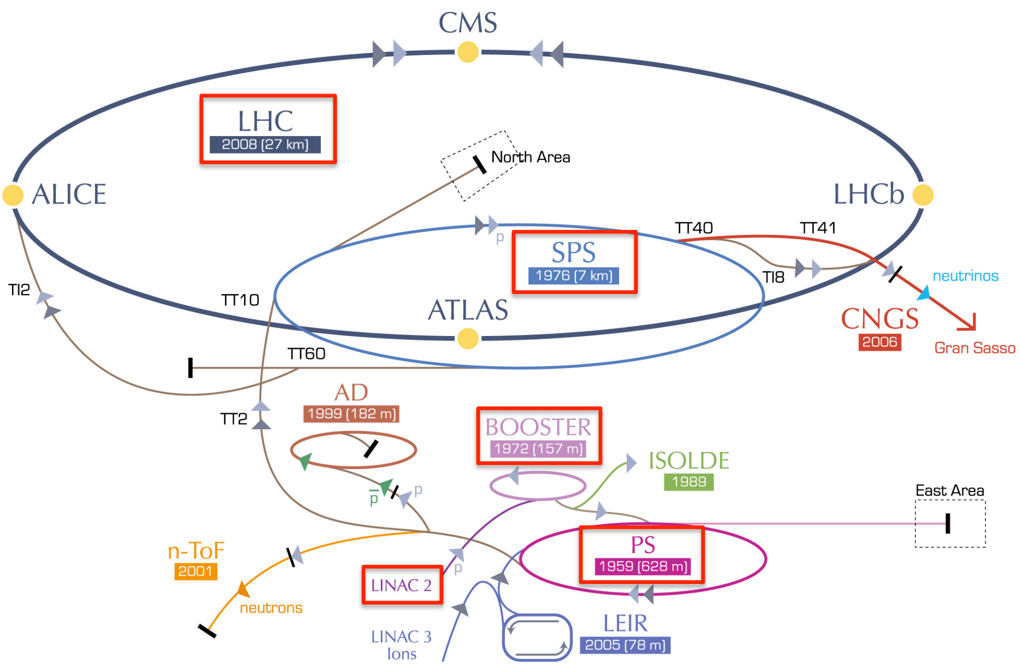

Fig. 4.1: CERN accelerator complex with the Linear Accelerator (LINAC 2), the Booster, the Proton Synchrotron (PS) and the Super Proton Synchrotron (SPS) as pre-injectors of the LHC. The LHC pre-injectors are marked with a red framing. [1]

dumped by the beam dumping system in IR6. A sketch of the underground layout with the caverns can be found in Figure 4.2.

4.2 The Experiments

The four major experiments in the LHC are called ATLAS, ALICE, CMS and LHCb and are optimised for different topics.

ATLAS and CMS are searching for new particles like the Higgs Boson and supersymmetry. They are the so-called high-luminosity experiments.

ATLAS (**A** **T**oroidal **L**HC **A**pparatu**S**) also looks for a possible substructure of the smallest particles like leptons and quarks. The detector measures the characteristic quantities of the produced particles in the collisions. The ATLAS detector is made from an inner pixel detector, a semi conductor tracker, a transition radiation tracker, an electro-magnetic and a hadronic calorimeter and a toroidial magnet system [4]. A schematic drawing of the ATLAS detector can be found in Figure 4.3.

The CMS (**C**ompact **M**uon **S**olenoid) detector searches for the Higgs Boson and, in addition, super-symmetric particles which may be helpful to explain dark matter in the universe. The CMS detector is made from an inner pixel detector, a semi conductor tracker, an electro-magnetic and a hadronic calorimeter and a big solenoid magnet [5].

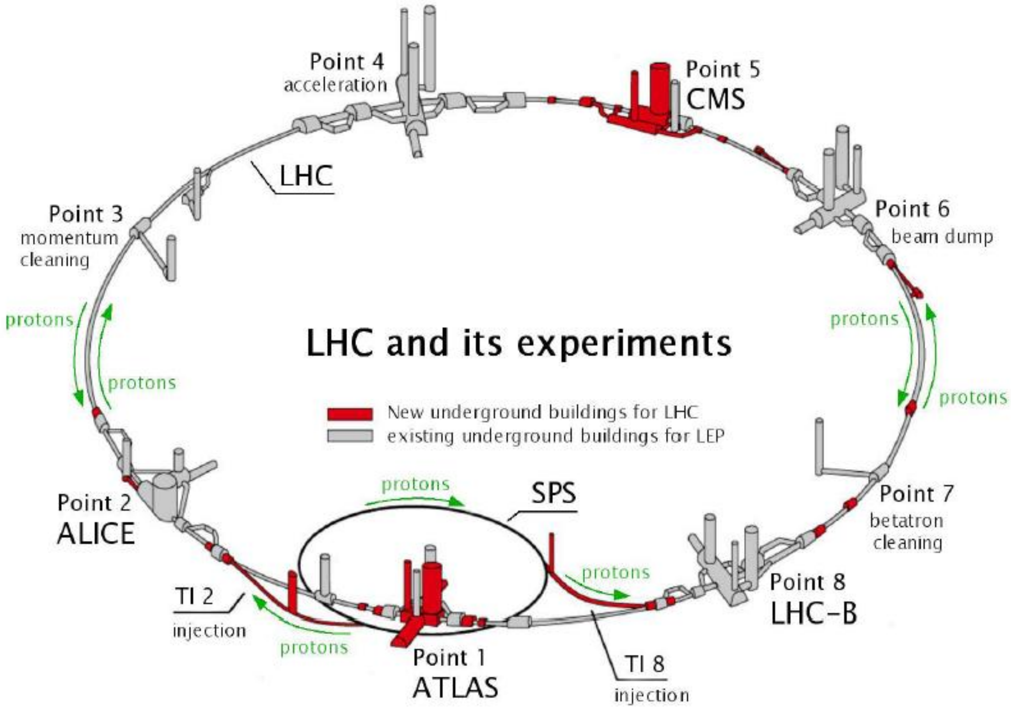

Fig. 4.2: Sketch of the underground layout of the LHC. Beam 1 circulates clockwise and beam 2 counter-clockwise. Collisions take place in the four interaction points of the experiments ATLAS (IP1), ALICE (IP2), CMS (IP5) and LHCb (IP8). Also the so-called cleaning insertions (Point 3 and Point 7), the dump section (Point 6), the acceleration insertion (Point 4), the transfer lines (TI 2 and TI 8) and the SPS (Super Proton Synchrotron) are shown. [3]

ALICE (**A** **L**arge **I**on **C**ollider **E**xperiment) studies the quark-gluon-plasma, an early state of the universe. ALICE includes an inner tracking system, a time protection chamber, a transition radiation detector, a time of flight detector, a high momentum particle identification detector, a photon spectrometer, a myon spectrometer and a surrounding magnet [6].
LHCb (**L**arge **H**adron **C**ollider **b**eauty) was especially designed to explore the asymmetry between matter and antimatter by studying the beauty quark. The components of LHCb are a vertex locator, trigger tracker, a surrounding magnet, tracking chambers, Cherenkov detectors, an electro-magnetic and a hadronic calorimeter and a myon spectrometer.

In addition to these four major experiments there are a few specialized smaller ones like TOTEM, ALPHA or LHCf [7].
The LHC delivers proton-proton collisions with a centre-of-mass energy of 7 TeV (2011), 8 TeV (2012) and 14 TeV nominal. The number of collisions in the experiments can be described by the so-called luminosity

$$L = \frac{N_b^2 n_b f_{rev} \gamma}{4\pi \epsilon_n \beta_z^*} F \tag{4.1}$$

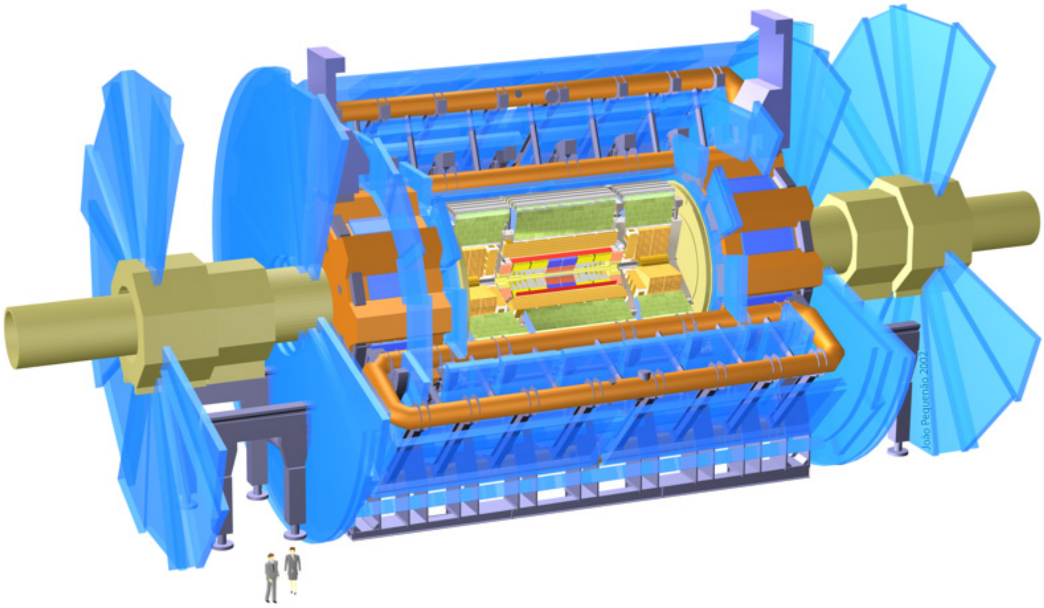

Fig. 4.3: Sketch of the ATLAS detector. One can see the different layers of the barrel-shaped detectors [4].

with the number of particles per bunch N_b, the number of bunches per beam n_b, the revolution frequency f_{rev}, the relativistic gamma γ, the transverse normalized emittance ϵ and the value of the beta-function at the IP β_z^*. A geometric correction F is necessary to take into account the luminosity reduction induced by the fact that the beams do not collide head-on but with a crossing angle [3].

In Table 4.1 the LHC beam parameters used in 2011 and the nominal LHC parameters are given [8, 9].

4.3 The Superconducting Magnet System

Only the use of superconducting magnets, which can transport a high current, can introduce magnetic fields that are necessary to bend and focus particles with such a high momentum as reached in the LHC. We have:

$$\vec{H} = \frac{\vec{B}}{\mu} \tag{4.2}$$

with the magentic field strenght $\vec{H}$, the magnetic flux density $\vec{B}$ and the permeability μ. The magnetic field strength is directly correlated to the current I in the magnets

$$H \sim I. \tag{4.3}$$

1232 main dipoles (MB), 386 main quadrupoles (MQ) and more than 4000 correctors are installed in the LHC tunnel. They operate at temperatures of 1.9 K and 4.5 K. A picture of the 15 m long dipole magnets (also called bending magnets) installed in blue cryostats in the LHC tunnel can be seen in Figure 4.4.

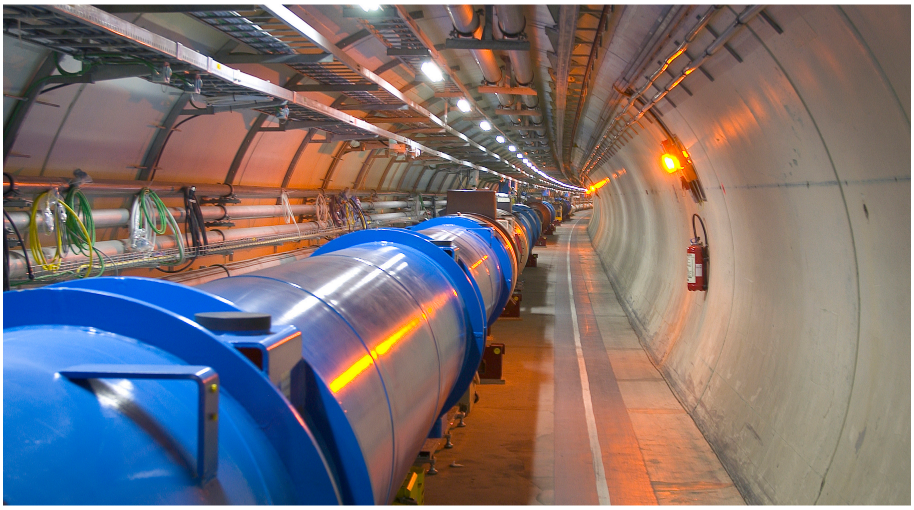

Fig. 4.4: LHC main bending magnet installed in the tunnel. [1]

The main bending magnets are made from niobium-titanium conductors with a surrounding copper matrix and reach a maximum magnetic field of 8.3 T at currents of 12.84 kA [10].

The main dipole magnets are used to keep the particles on their orbit around the machine. Quadrupole magnets are needed to focus the beams. In addition multipole magnets were installed to correct focussing errors (sextupoles) and higher multipole errors in the magnet system (octupoles, decapoles).

These superconducting magnets are very sensitive to heat released by particle losses. When the energy deposition reaches a limit of 5 mW/cm^3 the magnet will loose its superconductivity, called quench [11]. In this case the stored energy of the magnet is dissipated as heat and the beams are dumped.

4.4 The Cleaning Insertions

To handle the high stored energy of up to 362 MJ per beam in the LHC, it is essential to have a powerful cleaning system to avoid unnecessary quenches in the superconducting magnets. A comparison of the stored beam energy in previous and present proton storage rings is shown in Figure 4.5.

As seen in the previous section, the quench limit of the magnets is about 10 orders of magnitude lower than the stored energy. The quench limit was calculated to be reached with 7.6×10^6 lost protons per second and per meter at 7 TeV.

Therefore an efficient cleaning that intercepts these lost protons is necessary. The two types of cleaning are [13, 14]:

- The betatron cleaning in IR7 removes beam halo particles with too large amplitude in transverse betatron oscillations.

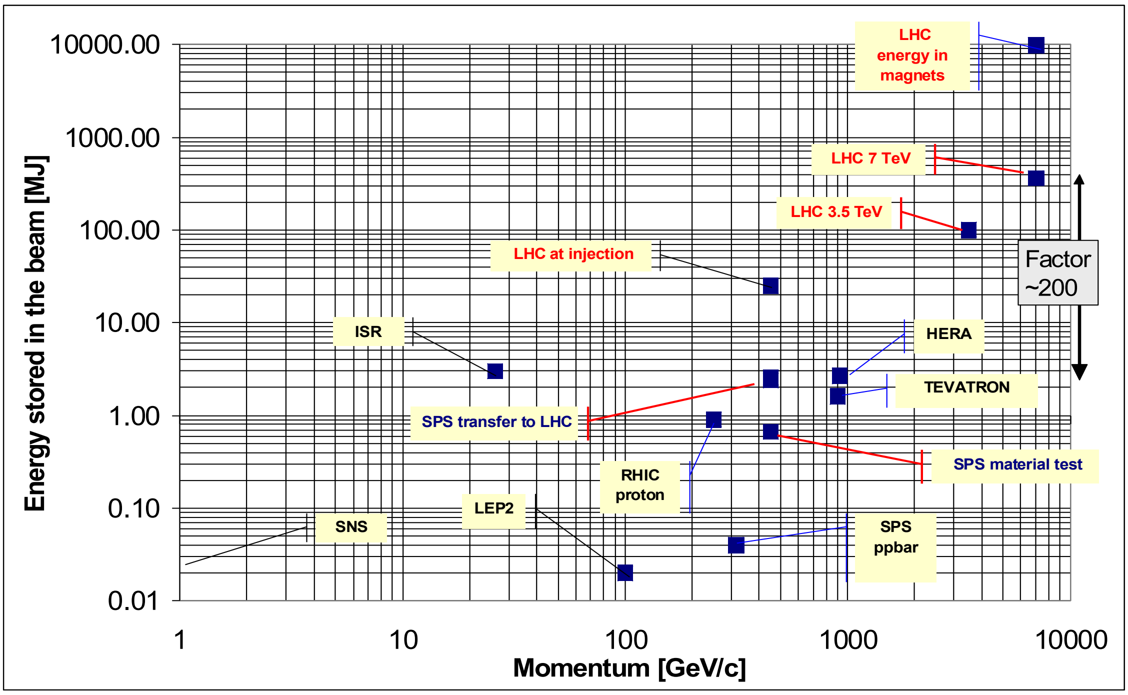

Fig. 4.5: Stored energy in storage rings. The main LHC parameters are labelled in red. One can see the beam momentum at injection (450 GeV), at top energy in 2011 (3.5 TeV) and at nominal operation (7 TeV). Also shown is the energy stored in the magnet system, compared to other accelerators. [12]

- The momentum cleaning in IR3 removes particles of the beam halo with too large energy offsets.

The collimation system of the LHC is described in detail in chapter 2.

4.5 Physics operation in the LHC

At the beginning of a fill a so-called pilot bunch ($\sim 1\times 10^{10}$protons) is injected into the LHC ring to guarantee the correct functioning of the magnet system. Only after this pilot bunch is circulating, the high intensity physics bunches (1.15×10^{11} p per bunch) can be injected. These physics bunches are normally injected in so-called trains. In 2011 the trains consisted usually of 144 bunches. With 50 ns bunch spacing a maximum number of 1380 bunches per beam was stored (nominal: 25 ns bunch spacing, 2808 bunches). The two beams are injected from the CERN **S**uper **P**roton **S**ynchrotron (SPS) with a particle momentum of 450 GeV.

After filling, the beams are ramped up to the final particle momentum (2011: 3.5 TeV, 2012: 4 TeV, nominal: 7 TeV). Thereby the current in the main dipole magnets is increased. The particles are accelerated with the help of 8 superconducting cavities installed in both beams. These cavities operate with an accelerating gradient of 5.5 MV/m and a frequency of 400 MHz [15]. During the ramp the parameters of the different systems (e.g. magnet current, collimator positions, etc.) are automatically driven by time dependent functions. At top energy the beams are then squeezed to arrive at the appropriate beta-function before they brought into collision in the experimental IPs. The operational mode when the beams collide is called *stable beams.*

After up to 14 hours of stable beams and luminosity production the beams are dumped, the magnets are ramped down, all systems are put to injection settings and a new fill can start. An overview of a physics fill is given in Figure 4.6. One can see the increase of the particle momentum (black) up to 450 GeV, then the injection of the two beams into the ring (blue for Beam 1 and red for Beam 2), followed by the ramp to 3.5 TeV. Then several hours of stable beams follow, after this, beam-dump and finally the ramp-down of the magnets at the end of the fill [16].

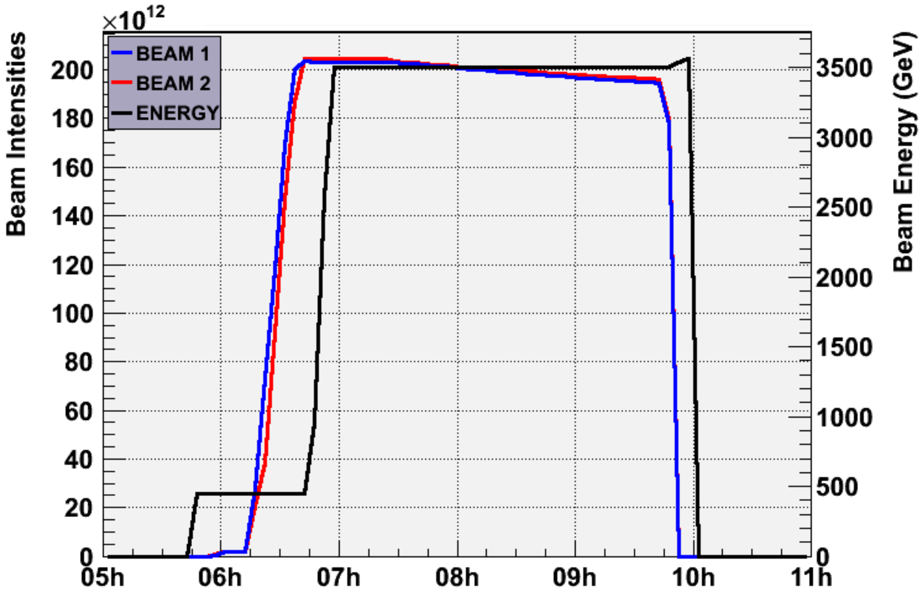

Fig. 4.6: Overview of the physics fill number 2266. The increase of the particle energy (black) to 450 GeV, then the injection of the pilot bunch and afterwards the injection of the two beams (blue for Beam 1 and red for Beam 2), followed by the ramp to 3.5 TeV, then 2.75 hours of stable beams, beam-dump and ramp-down of the magnets are shown.

During operation it is required to know the position of the beam in the vacuum pipe. This is achieved with the Beam Position Monitors (BPMs). Over 1000 of these monitors are installed in the ring [17].

Another important system is the Beam Loss Monitor (BLM) system to detect particle losses all around the ring. More than 3500 of these BLMs are installed in the LHC. These detectors are mainly ionization chambers [18]. Data from the BLM system have been intensively used in this thesis to calculate the particle loss rates at collimators. A detailed description of how these data have been used can be found in the chapter 6.

Tab. 4.1: Overview of beam parameters at injection, operation in 2011 and nominal operation with protons.

Protons	Injection	Collision (2011)	Collision (nominal)
Energy [GeV]	450	3500	7000
Relativistic gamma	479.6	3746	7461
Number of particles per bunch	1.15×10^{11}	$(1.15 - 1.55) \times 10^{11}$	1.15×10^{11}
Number of bunches per beam	1380	1380	2808
Stored energy [MJ]	23.3	110	362
Bunch spacing [ns]	25	50	25
Transverse normalized emittance [mrad]	3.75	3.75	3.75
Revolution frequency [kHz]	11.245	11.245	11.245
beta function in IP1 and IP5 [m]	11	1 - 1.5	0.55
beta function in IP2 [m]	10	10	10
beta function in IP8 [m]	10	3.5	1-50
Peak Luminosity in IP1 and IP5 [$cm^{-2}s^{-1}$]	-	3.5×10^{33}	1.0×10^{34}

4.6 Linear Beam Dynamics

This section will give an overview of linear beam dynamics in storage rings, which is essential to describe the motion of a charged particles in the LHC.

Equations of Motion

The forces, which determine the motion of a charged particle in a circular accelerator (or storage ring) are the Lorentz force F_l and the centrifugal force F_f in the horizontal plane

$$\vec{F_l} = q(\vec{v} \times \vec{B}) \tag{4.4}$$

$$F_f = m\, v^2/\rho. \tag{4.5}$$

where the charge of the particle is q, the velocity of the particle is $\vec{v}$, the magnetic flux density is $\vec{B}$, the mass of the particle is m and the bending radius is ρ. To keep the particle on its trajectory these forces need to be equal

$$F_f = F_l \tag{4.6}$$

Assuming $\vec{p} = m\vec{v}$ and $|\vec{v}| = \beta\, c$ with the relativistic parameter β and the speed of light c, this yields

$$\frac{1}{\rho} = \frac{e}{p} B_{vertical} \tag{4.7}$$

$$\rho = \frac{mc}{eB_{vertical}}. \tag{4.8}$$

Therefore particles in a circular accelerator are rotating on a fixed trajectory for every value of B. On every revolution they pass an accelerating longitudinal electrical field E which is produced by the RF in the cavities. The gain of energy between two points $\vec{r}_1$ and $\vec{r}_2$ is

$$\Delta E_{kin} = e \int_{\vec{r}_1}^{\vec{r}_2} \vec{E} d\vec{r} = e\, U \tag{4.9}$$

with U as the voltage in the cavities [19]. When a particle gets the momentum from the cavities, then the magnetic field has to be adjusted in the same way such that the trajectory of the particle remains unchanged. One can see that the acceleration is limited by the bending fields and the power of the cavities. One can also combine the two equations to obtain

$$\vec{F} = q(\vec{E} + \vec{v} \times \vec{B}) \tag{4.10}$$

and to describe the trajectory of a particle along a curved orbit in a circular accelerator. The coordinate s is introduced with a moving frame (x-y-coordinate) along this trajectory. In this case s describes the travelled distance and x and y are the transverse offsets at a certain point s. The reference frame is depicted in Figure 4.7.

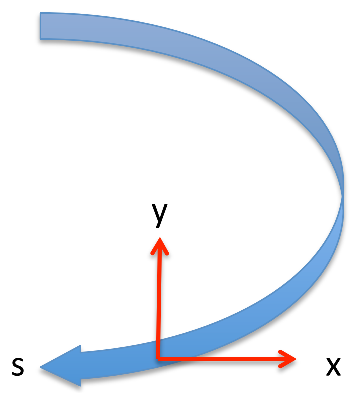

Fig. 4.7: Reference frame for a beam in a circular accelerator. The positive x-axis points outwards with respect to the ring.

Therefore one can describe a particle trajectory with the equation

$$\vec{r}(x(s), y(s)) = x\vec{e}_x(s) + y\vec{e}_y(s) + \vec{e}_s \tag{4.11}$$

with the normal vectors $\vec{e}_{x,y,s}$.

To get an individual particle trajectory one has to differentiate the vectors with respect to t

$$\dot{\vec{r}} = \dot{x}\,\vec{e}_x + \dot{y}\,\vec{e}_y + \left(1 + \frac{x}{\rho}\right)\,\dot{s}\,\vec{e}_s \tag{4.12}$$

The second derivative is given as

$$\ddot{\vec{r}} = \left[\ddot{x} - \left(1 + \frac{x}{\rho}\right)\frac{\dot{s}^2}{\rho}\right]\,\vec{e}_x + \ddot{y}\,\vec{e}_y + \left[\frac{2}{\rho}\,\dot{x}\,\dot{s} + \left(1 + \frac{x}{\rho}\right)\,\ddot{s}\right]\,\vec{e}_s \tag{4.13}$$

One can replace the time derivative by a derivative with respect to s. For the x-coordinate this yields

$$\dot{x} = \frac{dx}{ds}\frac{ds}{dt} = x'\,\dot{s} \tag{4.14}$$

$$\ddot{x} = x'\,\dot{s} + x'\,\ddot{s} = x''\,\dot{s}^2 + x'\,\ddot{s}. \tag{4.15}$$

The same was found for the other coordinates with this $\dot{\vec{r}}$ and $\ddot{\vec{r}}$ was evaluated

$$\dot{\vec{r}} = x'\,\dot{s}\,\vec{e}_x + y'\,\dot{s}\,\vec{e}_y + \left(1 + \tfrac{x}{\rho}\right)\,\dot{s}\,\vec{e}_s \tag{4.16}$$

$$\ddot{\vec{r}} = \left[x''\,\dot{s}^2 + x'\,\ddot{s} - \left(1 + \tfrac{x}{\rho}\right)\tfrac{\dot{s}^2}{\rho}\right]\,\vec{e}_x + \left(y''\,\dot{s}^2 + y'\,\ddot{s}\right)\,\vec{e}_y + \left[\tfrac{2}{\rho}\,x'\,\dot{s}^2 + \left(1 + \tfrac{x}{\rho}\right)\,\ddot{s}\right]\,\vec{e}_s \tag{4.17}$$

This yields with $\dot{\vec{p}} = m\,\ddot{\vec{r}}$ and $\vec{v} = \dot{\vec{r}}$ to

$$\ddot{\vec{r}} = \frac{e}{m}\,\left(\dot{\vec{r}} \times \vec{B}\right). \tag{4.18}$$

With the fact that the magnetic field has only transversal components $B_s = 0$ and with the approximation $\ddot{s} \approx 0$ one can find

$$x''\,\dot{s}^2 - \left(1 + \frac{x}{\rho}\right)\frac{\dot{s}^2}{\rho} = -\frac{e}{m}\,B_y\,\left(1 + \frac{x}{\rho}\right)\,\dot{s} \tag{4.19}$$

$$y''\,\dot{s}^2 = \frac{e}{m}\,B_x\,\left(1 + \frac{x}{\rho}\right)\,\dot{s}. \tag{4.20}$$

With the equation $p = m\,v$,

$$v = \dot{s}\,\frac{\rho + x}{\rho} = \dot{s}\,\left(1 + \frac{x}{\rho}\right) \tag{4.21}$$

and the inverse momentum

$$\frac{1}{p} = \frac{1}{p_0}\left(1 + \frac{\Delta p}{p_0}\right). \tag{4.22}$$

One can evaluate

$$\frac{e}{p_0}\,B_y = \frac{1}{\rho} + k_0\,x \tag{4.23}$$

$$\frac{e}{p_0}\,B_x = k_0\,y \tag{4.24}$$

with k_0 being the regular normalized magnetic gradients of the focussing magnets of an accelerator. Assuming $x \ll \rho$ and $y \ll \rho$, this leads to the equation of motion for a charged particle in a circular accelerator [19]

$$x''(s) + \left(k_0(s) + \frac{1}{\rho_0^2(s)}\right)\,x(s) = \frac{1}{\rho_0(s)}\,\frac{\Delta p}{p_0} \tag{4.25}$$

$$y''(s) - k_0(s)\,y(s) = 0. \tag{4.26}$$

4.7 Transverse Motion

Using u for the transverse coordinates x or y, $k_u(s)$ for the corresponding focussing function and assuming

$$\frac{\Delta p}{p_0} = 0$$

the equation of motion can be generalized to the so-called Hill‘s equation

$$u''(s) + k_u(s)u(s) = 0 \tag{4.27}$$

with $k_u(s + L) = k_u(s)$ and the circumference of the circular accelerator L. U(s) describes the oscillation of the particles around the orbit. The amplitude and the phase of this oscillation are functions of the position s. This oscillation is called transversal betatron-oscillation. The solution of equation 3.27 can be found with the ansatz

$$u(s) = \sqrt{A_u\beta_u(s)}sin(\mu_u(s) + \mu_{u_0}) \tag{4.28}$$

with the amplitude A_u and the amplitude modulation of the oscillation $\beta_u(s)$ in the according plane (x,y). $\beta_u(s)$ is also known as the betatron function and $\mu_u(s)$ and

μ_{u_0} as phase advance of this oscillation, respectively the initial phase of the betatron oscillation, defined as

$$\mu_u(s) = \int_0^s \frac{ds}{\beta_u(s)}. \tag{4.29}$$

One can substitute the amplitude A_u by the constant ϵ, the so-called emittance. Particles in the focussing magnet structure in a storage ring perform oscillation with the position-dependent amplitude

$$E(s) = \sqrt{\epsilon\,\beta(s)}. \tag{4.30}$$

E (s) can be interpreted as envelope of the particle movement in a circular accelerator.

The derivative of the solution of the Hill's equation delivers the equation for the emittance ϵ

$$\beta_u(s)(u'(s))^2 + 2\alpha_u(s)u(s)u'(s) + \gamma_u(s)u^2(s) = \epsilon \tag{4.31}$$

α_u, β_u and γ_u are the so-called Twiss parameters and depend on β_u

$$\begin{aligned} \alpha_u(s) &= -\frac{1}{2}\,\beta_u'(s) \\ \beta_u(s) & \\ \gamma_u(s) &= \frac{1+\alpha_u^2(s)}{\beta_u(s)} \end{aligned} \tag{4.32}$$

In the phase space, the map of a particle trajectory at any given position s is represented by an ellipse with the surface area $\pi\epsilon$. Liouville's theorem states

$$\pi\epsilon = constant \tag{4.33}$$

if the particles are under the influence of conservative forces Another important parameter to describe beam dynamics is the machine tune.

$$Q = \frac{1}{2\,\pi}\int_0^L \frac{ds}{\beta_u(s)}. \tag{4.34}$$

The tune is the number of betatron oscillations per turn. One can also define the tune spread

$$\Delta Q_z = \xi\frac{\Delta p}{p} \tag{4.35}$$

with the gradient error in the magnetic field of the magnets, the so-called chromaticity ξ [13, 19].

4.8 LHC Aperture

The geometric aperture A_{geom} is the aperture given by the mechanical openings of the equipment of the circular accelerator (e.g. beam pipe, collimators).
A picture of the LHC beam pipe is given in Figure 4.8. The aperture is generally given in units of the beam size, as defined by:

$$\sigma_u(s) = \sqrt{\beta_u(s)\epsilon_{rms} + \left(D_u(s)(\frac{\Delta p}{p_0})_{rms}\right)^2}. \tag{4.36}$$

β_u (s) is the betatron function in the corresponding plane, ϵ_{rms} is the beam emittance and $D_u(s)$ is the dispersion function.

The so-called beam acceptance of a circular accelerator is defined as:

$$C_u(s) = \frac{(A_{geom}(s)\sigma_u(s))^2}{\beta_u(s)}. \tag{4.37}$$

$C_u(s)$ is the maximum area, directly related to the geometric aperture, which can be covered by the phase-space ellipse at any location of the accelerator. Higher order magnets cause non-linear perturbations of the particle motion. Due to these non-linearities the so-called dynamic aperture can be defined.
Particles with a larger amplitude than the dynamic aperture will be lost in the aperture bottlenecks, mainly defined by the collimators. In the LHC the dynamic aperture bottleneck in σ at top energy in 2011 is given with 5.7 σ at the primary collimators [3].

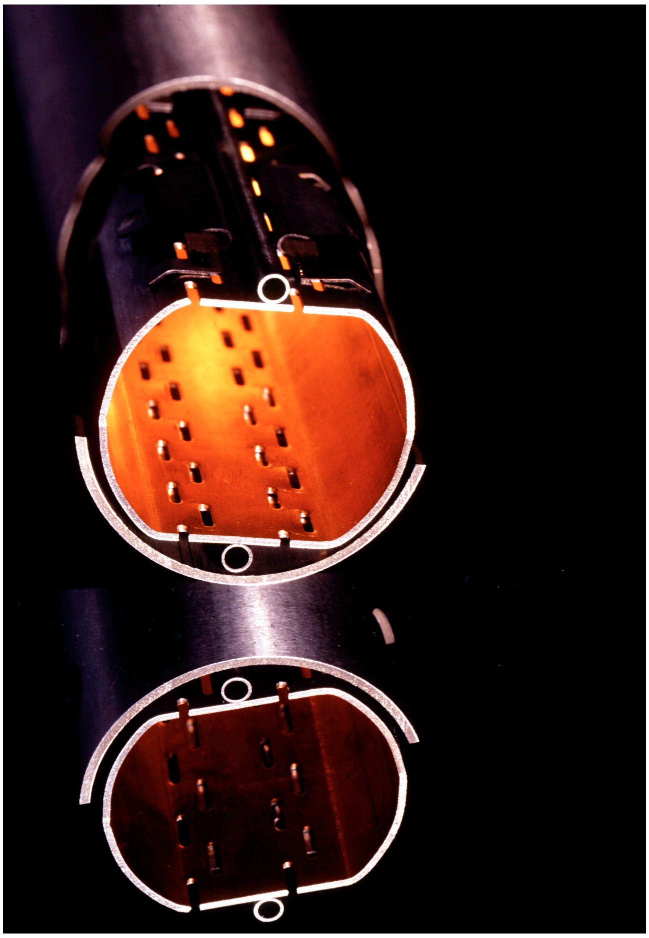

Fig. 4.8: Picture of the LHC beam pipe with an average diameter of 56 mm. The inner and outer tube is shown. [1]

5. THE LHC COLLIMATION SYSTEM

Due to the high risk of damaging the LHC with the particle beams the LHC collimation system was installed. In this chapter the collimation system presently installed in the LHC is introduced and an outlook to future upgrades will be given.
In the second part of this chapter the required performance of the LHC collimation system will be briefly explained.

5.1 Collimation in the LHC

Due to high intensities ($I_{nom} \sim 3e14\,p$) and the beam momenta ($E_{nom} = 7\,TeV/c$) combined with the application of superconducting magnets the LHC requires a sophisticated collimation system. This is necessary to protect the magnet system from unavoidable beam losses.
The major parts of the collimation system are placed in the long straight sections of IR3 and IR7. IR3 is dedicated to momentum and IR7 to betatron cleaning. In addition, several protection devices are installed in the LHC ring, for example at the injection and extraction points and upstream of the four main experiments.

Three different materials (carbon, copper and tungsten) and settings for various types of collimators depending on their function are used.

5.1.1 Challenges for the LHC Collimation System

The LHC collimation has to handle

- High stored energy and intensity
  With the high number of bunches (2808 per Beam), the high intensity ($\sim 3e14\,p$ per beam) and the high beam momentum (7 TeV) this yields a stored beam energy of 350 MJ. Note, with this power it is possible to melt 420 kg of Copper.

- Superconducting magnet environment
  Protons can get lost into the cold aperture, therefore heat is deposited in the magnet and the magnet can quench. This requires a high cleaning efficiency of $\geq 99.999\%$.

- Tight collimation settings
  During normal operation the primary collimator is placed at 5.7 σ at top energy the sigma is given with $\sigma = 0.2\,mm$. This corresponds to a opening of $\sim$ 2.3 mm [14, 20].

Therefore the collimation system of the LHC has been designed to provide:

- Cleaning of the particle losses due to the continous population of the beam halo with sufficient efficiency ($\geq$ 99.999 %) to avoid quenches in the superconducting magnets.
- Passive machine protection to protect the machine against regular and irregular losses induced by equipment failures.
- Minimization of collimation-related background at the experiments to ensure clean data acquisition.
- Handling of beam-induced radiation effects on electronics.

[13, 14, 21]. It was decided to use a phased approach in the installation of the LHC collimation system.

5.1.2 Phase 1 Collimation System

The so-called phase 1 collimation system is currently installed in the LHC and used through the whole cycle of the machine operation (injection, top energy, collision). It consists of 88 movable collimators, installed in the ring (44 per beam) and 14 in the transfer lines to the LHC. It is a four-stage system. The main devices are primary (TCP), secondary (TCSG) and tertiary (TCT) collimators. 5 Absorbers (TCLA), collimators in the injection regions (TCLI and TDI) and in the extraction regions (TCDQA) complement the collimation system in the LHC. The TCTs are installed upstream of the experimental IRs to protect the triplet magnets, which perform a strong focussing of the particle beams into the IPs. Special absorbers are placed downstream of the IPs to collect the debris from physics operation. Per beam this number of collimators was installed in IR3

- 1 primary collimator (horizontal)
- 4 secondary collimators (horizontal)
- 4 absorbers (horizontal, vertical)

and in IR7

- 3 primary collimators (horizontal, vertical, skew (tilted by an angle of 127 degrees))
- 11 secondary collimators (horizontal, vertical, skew)
- 5 absorbers (horizontal, vertical)

and 8 tertiary collimators (2 per experimental IP).
An overview of all collimators in the LHC in given in Figure 5.1 and a sketch of the four-stage collimation system is depicted in Figure 5.2.

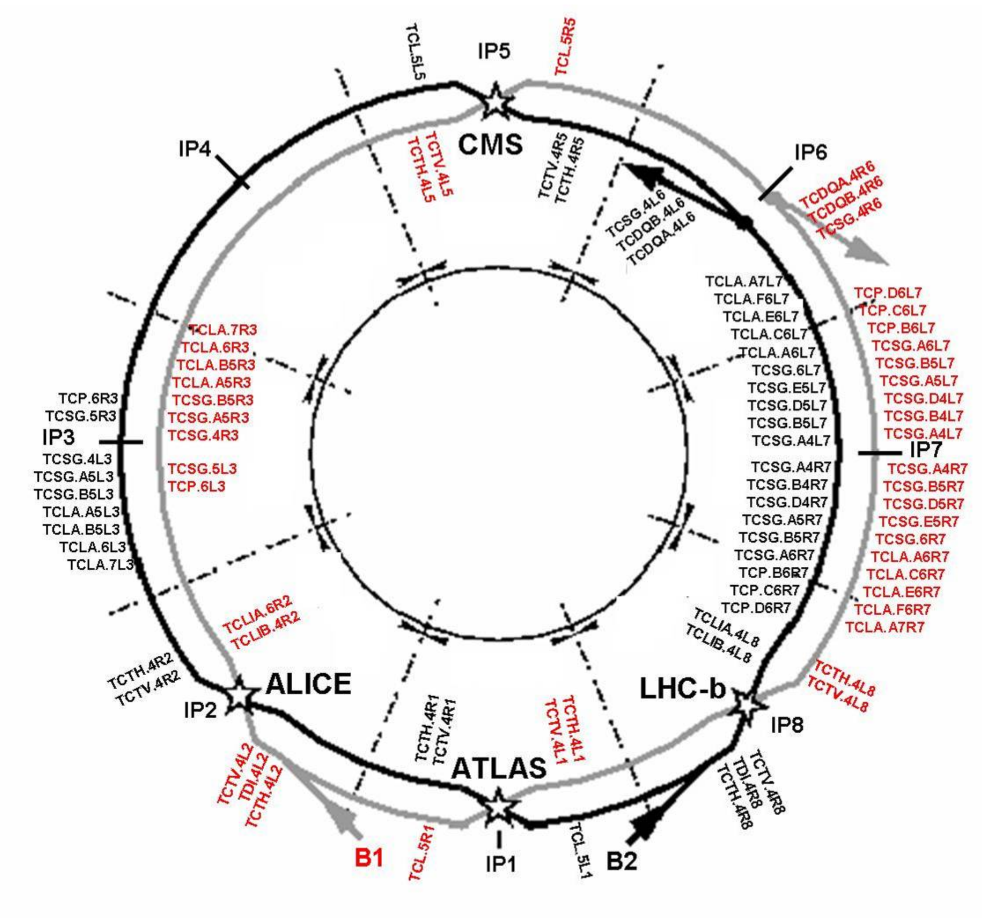

Fig. 5.1: Sketch of the layout of the present phase-I collimation system. Beam 1 (beam 2) collimators are shown in red (black). The major part of the collimators in IR3 (momentum cleaning) and in IR7 (betatron cleaning) [13].

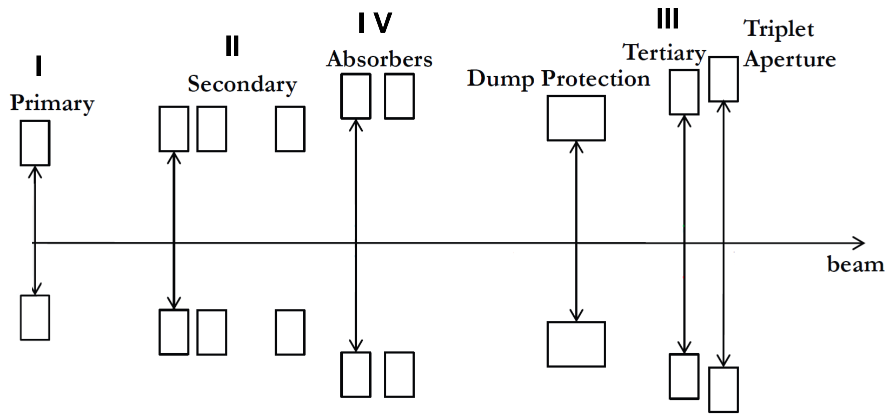

Fig. 5.2: Principal sketch of the four-stage cleaning system. The TCPs closest to the beam followed by the TCSGs and absorbers and the TCTs in front of the experimental triplet magnets [22].

Tab. 5.1: Collimator settings in unit sigma for top energy in 2011 and for nominal energy.

Collimator family	Top energy (2011) [σ]	Top energy (nominal) [σ]
TCP-IR7	5.7	6.0
TCSG-IR7	8.5	7.0
TCLA-IR7	17.7	10.0
TCTs in IP1/5/8	11.8	8.3
TCSG-IR6	9.3	7.5
TCDQ-IR6	9.8	8.0

In Table 5.1.2 one can find the collimator settings for 2011 and for nominal operation. In a collimator-setup the jaws are centered around the beam. This is required for new settings in the machine, e.g. new values for the beta-function, new energy. In addition the jaw opening must be variable to the changes in the beam size as a function of the energy. Therefore the collimator jaws are driven by functions during the ramp.

5.1.3 Collimator Types and Materials

In the LHC a collimator is made from two movable jaws. Four stepping motors move them with a maximum speed of 2 mm/s and a minimal stepsize of 5 μm.

The collimator jaws are made from different materials, like carbon-fibre-reinforced carbon composites for the TCPs and Tungsten for the TCTs. The jaws are water cooled to conduct the heat load of impacting protons. The jaws have an active, flat part, a tapering and RF-fingers, which provide contact for the radio-frequency fields and currents between collimator and vacuum flanges, at both ends. Figure 5.3 and Figure 5.5 show pictures of a secondary collimator. With an opened vacuum tank, one can see the jaws, the RF-fingers, also the cooling pipes and the jaw opening during assembly.

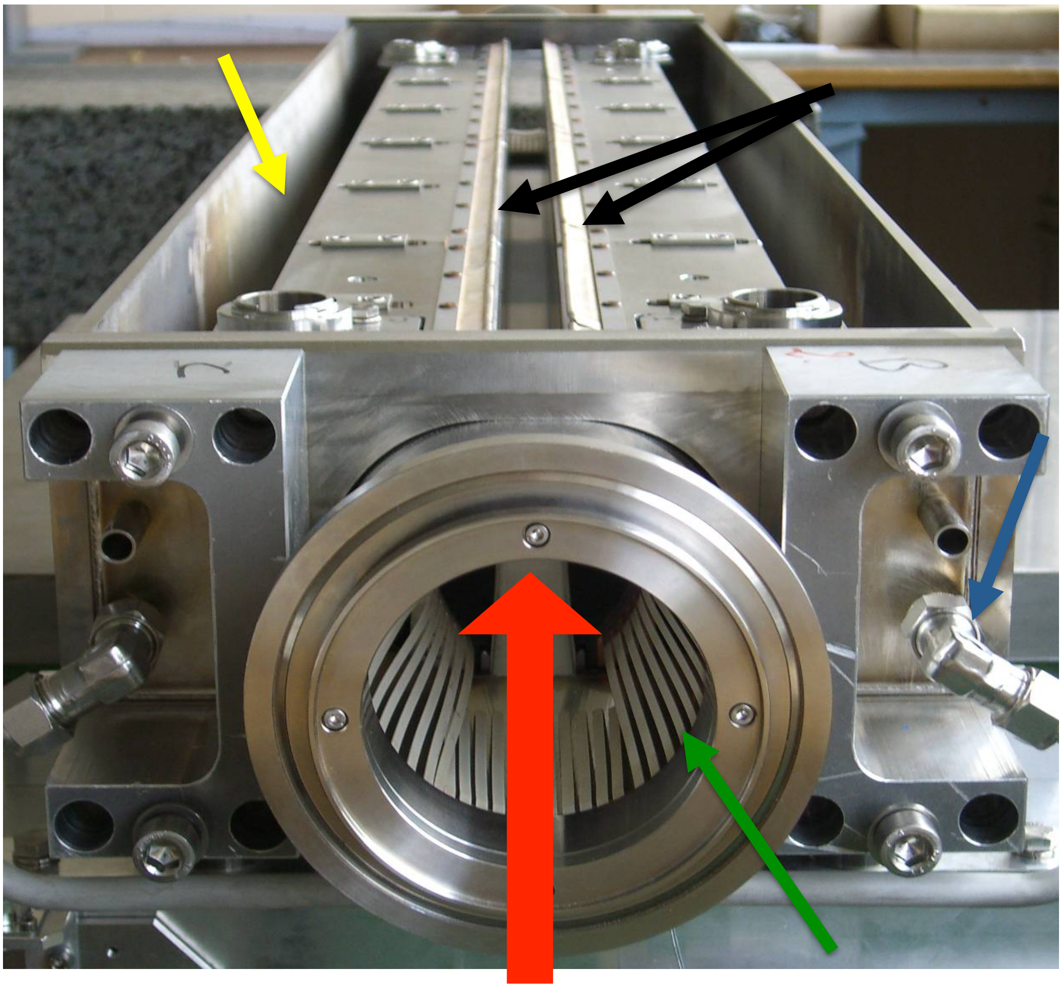

Fig. 5.3: Picture of the 1.2 m long TCSG collimator. One can see the beam direction (red arrow), the connection to the water cooling (blue arrow), the RF-fingers (green arrow), the two jaws (black arrows) who are mounted in the vacuum tank (yellow arrow) [23].

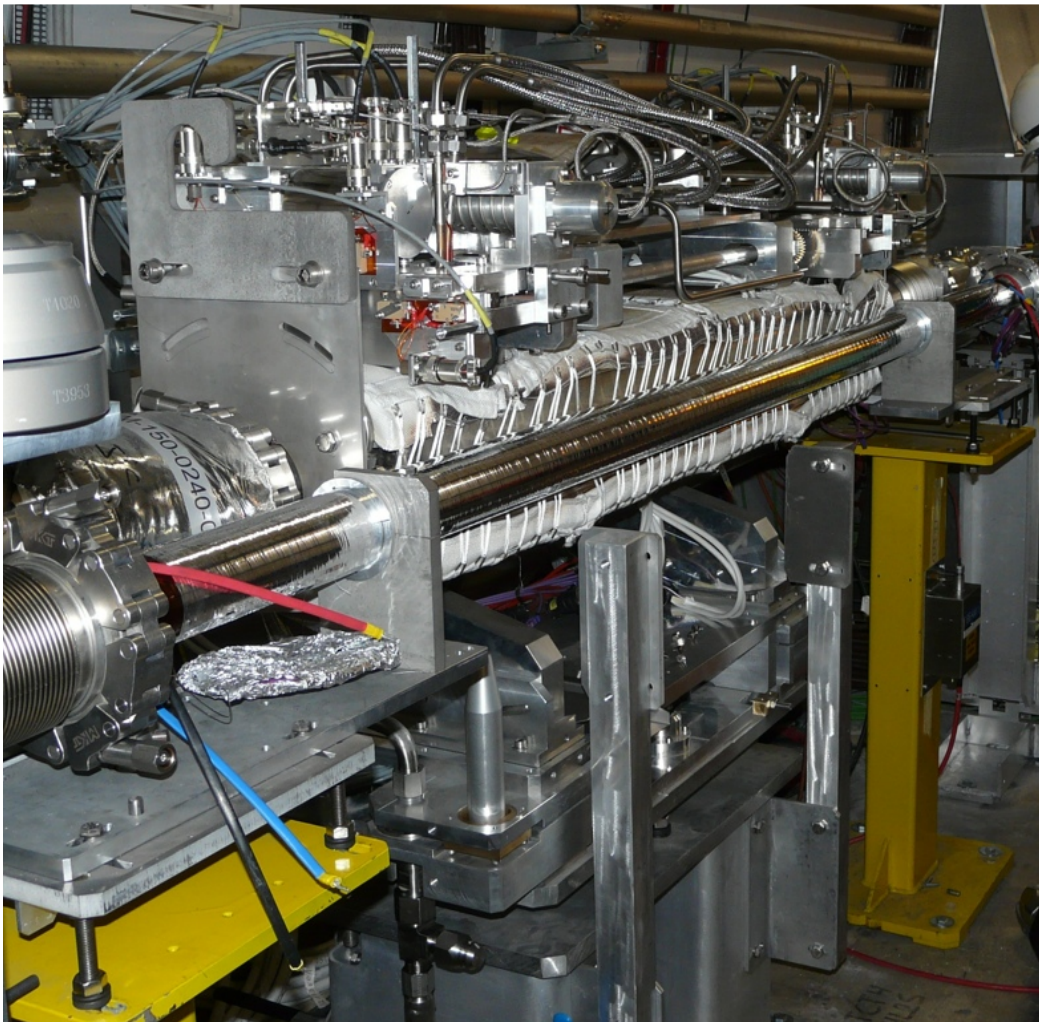

Fig. 5.4: Picture of tertiary collimator installed in IP2. In front one sees the beam pipe for the other beam 1 and in the back the collimator for beam 2 [23].

Tab. 5.2: Functional requirements for the main collimators in the LHC.

Parameter	TCP	TCSG	TCLA / TCT
Material	C or C-C	C or C-C	W
Jaw length [m]	0.6	1.0	1.0
Maximum gap [mm]	60	60	60
Minimum gap [mm]	0.5	0.5	0.5
Gap size precision [μm]	50	50	50
Jaw position control [μm]	≤ 10	≤ 10	≤ 10

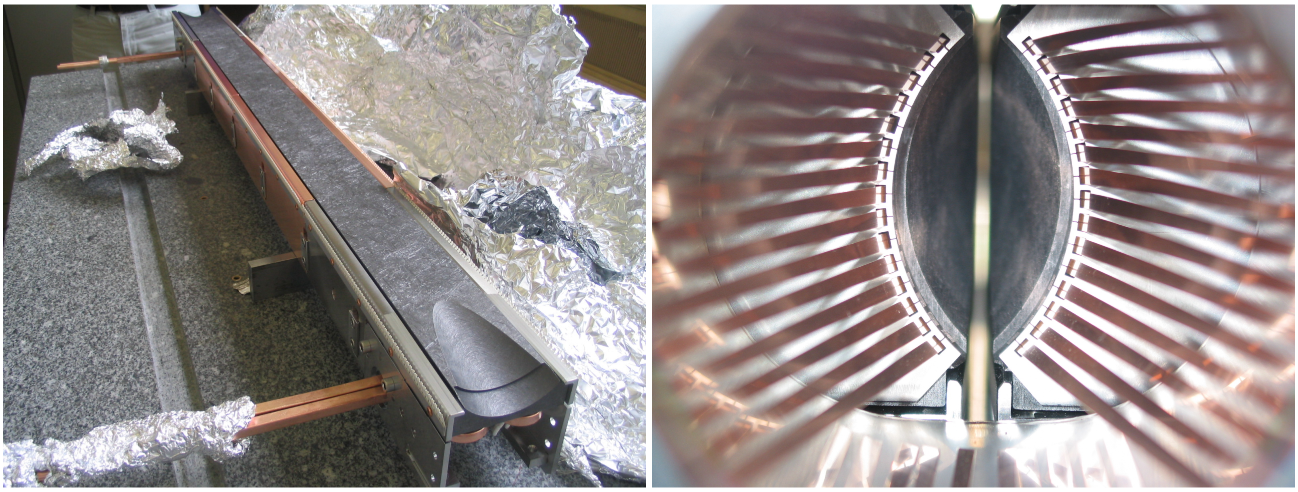

Fig. 5.5: **Left**: Top view of a secondary collimator jaw during assembly. One can see the flat part in the middle, the tapering on both ends and the copper cooling pipes. **Right**: Front view of a collimator with the RF-fingers. The jaw opening of a few mm is shown [23].

The requirements for the collimator jaws are defined as such [14]:

- The collimators jaws have to withstand beam impacts of up to 500 kW deposited energy.
- The surface of a jaw must remain flat on the 10-25 μm level.
- The collimation system must have the required cleaning efficiency.
- The choice of materials must be acceptable regarding impedance.

To find a good compromise between particle absorption, robustness and impedance, carbon-reinforced material was used for the primary and secondary collimators, which require the highest robustness.
The tertiary collimators and the absorbers are made of tungsten jaws, because they have to absorb the tertiary halo and the particle showers from the primary and secondary collimators [25, 26]. An overview of the different materials and lengths of the collimators is given in Table 5.1.3. .

5.1.4 Future Types of Collimators

The phase 1 collimation system was designed for maximum robustness even if this implies lower cleaning efficiency by using the robust low Z materials for the TCPs and TCSGs. In the next step, the phase 2, a set of additional secondary collimators will be installed in the LHC. The new collimators will have a higher cleaning efficiency by using higher Z materials, but they will be less robust. Using low impedance hybrid materials these collimators will upgrade the collimation system. In the LHC there are 50 places reserved for these new collimators [27].

Other future types of collimators are the rotating collimators, hollow-electron-beam lenses and collimators with Beam Position Monitors in the jaws. Also new collimation schemes like the crystal collimation will be tested. These future directions are currently under investigation. For this, CERN is working in collaboration with several other laboratories, like SLAC, FNAL, BNL or EPFL [28, 29] . In the far future, additional collimators have to be installed near the high-luminosity IPs to absorb the collision debris downstream of the experiments.

5.2 Required Performance of the LHC Collimation System

To deliver the nominal design luminosity it is necessary to store beams of up to 360 MJ in the superconducting ring of the LHC. The loss of only a fraction of 10^{-3} of the beam at top energy over 10 seconds can cause a quench in the superconducting magnet system. This requires a highly efficient performance of the LHC collimation system to intercept and safely absorb losses and protect the LHC from avoidable quenches.

To deliver the high efficiency, the gap opening of the collimators has to be small, but in addition, the collimator should not intercept the core of the beam and increase the impedance by putting materials too close to the beam.

The losses should mainly be intercepted by the primary collimators, which are supposed to be the aperture bottleneck of the LHC. In the concept of a collimator hierarchy the primary collimators have to stay closest to the beam, followed by secondary collimators. With a small retraction between secondary and primary collimators (only 2.8 in units of beam sigma) this makes tight tolerances and excellent movement control necessary [25].

5.2.1 Beam Loss

In circular accelerators particles are distributed in a beam core and the surrounding area, called beam halo, which is limited by the aperture. The stable trajectory where a particle can perform a large number of turns is limited by the dynamic aperture. Particles outside of the dynamic aperture get lost. In the LHC they should get lost at the collimators. A particle can be kicked out of the dynamic aperture by various reasons. These processes create the beam halo and are called regular losses. Regular losses are unavoidable and make cleaning necessary to minimize their effect on the elements of the machine. [13, 21] The reasons which induce these regular losses are listed here:

- Intra-Beam scattering.
- Touschek scattering.
- Scattering on residual gas molecules.
- Emittance growth through multiple coulomb scattering.
- Synchrotron radiation.
- Beam-Beam interaction.

Irregular losses can be produced by unexpected or failure cases. Theses failures can cause high losses on the timescale of a couple of LHC turns ($\sim 100\,\mu s$). Examples for these are:

- Injection errors.
- Failure of kicker magnets.
- Failure of RF system.

Other failure cases which can cause irregular losses but on longer timescales are:

- Vacuum loss.
- Failures in the powering of the magnets.
- Wrong operational action, like tune trims, orbit corrections, etc.

5.2.2 Cleaning Inefficiency

The particles which are not lost in the collimator jaws can hit the cold aperture of the machine and induce a quench of the affected superconducting magnet. The cleaning performance of a collimation system is described by the cleaning inefficiency. The cleaning inefficiency is given by the ration of particles that reach a normalized amplitude A_{cut} which corresponds to the machine aperture A_r over the total number N of particles impacting on a primary collimator

$$\eta_c(A_{cut}) = \frac{1}{N} \sum_{i=0}^{N} H(A_r(i) \; - \; A_{cut}) \tag{5.1}$$

where $A_r(i) = \sqrt{A_x^2(i) + A_y^2(i)}$ is the radial amplitude of the ith particle and H is the Heaviside step function returning 1 when $A_r \geq A_{cut}$ and 0 otherwise. [21].

This ratio will give the leakage rate from the primary collimators to the superconducting areas. During normal physics operation at top energy, it is required that η_c is below 10^{-3}. This means that 99.9 % of the protons are absorbed in the collimators.

Highly concentrated local losses can cause quenches, even if the global cleaning efficiency is as required. Therefore the local cleaning inefficiency is defined as

$$\eta_{c,local} = \frac{\eta_c}{L_{dil}}, \tag{5.2}$$

with the dilution length L_{dil}. [13, 21, 22]

5.2.3 Quench Limits

For transient losses on the timescale of a couple of LHC turns ($\sim 100\,\mu s$) the number of protons N_q to quench a magnet is described by:

$$N_q = \frac{\Delta Q_c}{t}. \tag{5.3}$$

ΔQ_c is the amount of heat per unit volume, which is necessary to increase the temperature in the superconducting coils above the transition temperature. The heat introduced by continuous losses needs to be continuously compensated by the cryogenic system.

The energy of the lost protons will be diluted over the length L_{dil}. The local loss rate $R_{q,local}$ which would induce a quench can be calculated as

$$R_{q,local} = \frac{R_q}{L_{dil}}. \tag{5.4}$$

The maximum local loss rate can be re-defined as:

$$R_{q,local} = 1.7 \ \times 10^8 [p/s]\, E^{-\frac{3}{2}} \tag{5.5}$$

with the particle momentum in TeV/c. The maximum loss rate at the primary collimators is then described by

$$R_{loss} = \frac{R_q}{\eta_{c,local}} \tag{5.6}$$

with the quench limit R_q and the local cleaning inefficiency $\eta_{c,local}$. [11, 13, 21]

5.2.4 Instantaneous Loss Rates and Beam Lifetime

To deliver a high integrated luminosity it is necessary to have a beam lifetime which is high enough to have several hours of stable beams per fill. Therefore the level of losses and as a consequence the beam lifetime becomes an important parameter. The evaluation of the beam intensity as a function of time can be described by

$$N_p(t) = N_0 \ exp(-t/\tau). \tag{5.7}$$

with the beam intensity $N_p(t)$ at t, the initial intensity N_0 and the beam intensity lifetime τ. The beam intensity lifetime τ is defined as the time needed to reduce the number of particles by a fraction of 1/e of the initial intensity. With the usage of a series expansion of Equation 5.7 the beam lifetime for small losses can be directly calculated from the loss rate R_{loss}

$$\tau(t) \approx \frac{N_{tot}}{R_{loss}(t)}. \tag{5.8}$$

One can see that instantaneous losses cause a decrease of the beam lifetime. To get a beam lifetime which is large enough for the required production of integrated luminosity it is necessary to keep losses under a certain limit. A detailed describtion of the lifetime evolution during one fill can be found in the chapter 9.

6. QUALIFICATION OF THE LHC COLLIMATION SYSTEM

The required cleaning inefficiency has to be controlled during the run of the LHC. Therefore a system for its qualification was developed. In this chapter one can find an introduction to the method used to qualify of the LHC collimation system. The betatron and momentum cleaning inefficiencies are analysed for the first half of 2011. Then the calibration factor for collimators, losses at the collimators and loss maps in Watt are discussed.

6.1 Betatron and momentum cleaning inefficiency

As discussed in chapter 5.1 the collimators installed in IR3 are currently used to clean off-momentum particles, the collimators in IR7 to catch particles with a too large betatron amplitudes. The collimation system has a hierarchy, where the primary collimators cut the beam halo. The secondary collimators intercept the secondary halo (mainly protons, but also shower particles like pions, electrons) and the absorbers catch the particle showers produced at the jaws of the Collimators and the tertiary halo.

The performance, i.e. the hierarchy and the local cleaning inefficiency, the settings of the system and its stability have to be controlled and verified regularly to ensure maximal cleaning inefficiency and protection. This qualification is performed with the so-called loss maps. These loss maps have to be performed for each change in collimator settings. [30, 31]

For generating loss maps multi-turn beam losses are induced. This means that particles get lost over several turns in the machine. For betatron cleaning this is done by crossing the one-third integer tune resonance. Therefore the betatron amplitude of the particle is increased and the particle hits a collimator. With this method one can create horizontal and vertical losses to monitor the horizontal and vertical cleaning inefficiency.

Off-momentum loss maps are performed by changing the RF-frequency by $\pm$ 1000 Hz. This changes the momentum of the particles and they are mainly lost at IR3 collimators.

To minimize the risk of machine damage during the qualification, but still guarantee a proper resolution and orbit one nominal bunch ($\sim$ 1.15e11 p) is used.

For the analysis the losses measured by beam loss monitors are plotted along the whole machine, normalized to the highest loss at the primary collimators. Thus, the measured local cleaning inefficiency is defined as

$$\eta_{c,i}^{meas} = \frac{R_i}{R_{i,max}}. \tag{6.1}$$

Figure 6.1 shows a betatron loss map around the full ring, while Figure 6.2 shows a zoom in IR7.

To achieve this type of plot the following steps had to be performed:

- Extract the signals from the logging database.
- Evaluate exact time stamp of the highest loss rate.
- Evaluate a part before losses were generated, preferably without beam for offset subtraction.
- Normalize the BLM signals to the highest signal (normally at a primary collimator in IR3 or IR7).
- Plot the local cleaning inefficiency with a color-labeling for collimators (black), warm magnets (red) and cold superconducting aperture (blue).
- Plot special zooms for regions downstream of an IR and label the magnets in these sensitive areas.

This betatron loss map in the horizontal plane for Beam 2 shows the typical shape of a betatron loss map. The highest cleaning inefficiency can be found at the collimators in betatron cleaning insertion IR7 followed by the collimators in dump section IR6 ($\eta = 8 \times 10^{-3}$) and the off-momentum cleaning in IR3 ($\eta = 5 \times 10^{-3}$). For the tertiary collimators around the experiments in IR1, IR2, IR5 and IR8 a cleaning inefficiency of 1×10^{-6}, and in IR1 up to 3.5×10^{-5} in IR5 was evaluated. During this loss map 9.1×10^{11} protons got lost within 1 second.

The zoom in IR7 shows the hierarchy of the LHC collimation system. The highest cleaning inefficiency can be found at the primary collimator. Then the cleaning inefficiency decreases exponentially from the TCPs down to the TCLAs. The highest cleaning inefficiency in the cold region was evaluated with 6.7×10^{-4} at the Quadrupole Q8 downstream of IR7.

Afterwards an off-momentum loss map was performed. The RF-frequency was increased by 1000 Hz and the loss map was performed with both beams in parallel. In this case the highest loss occurred, as expected, at the primary collimators in IR3. The local cleaning inefficiency around the ring is plotted in Figure 6.3 and a zoom in the off-momentum cleaning insertion IR3 is depicted in Figure 6.4.

The cleaning inefficiency was monitored during the run in 2011. In Figure 6.5 the highest cleaning inefficiency at a superconducting magnet (Q8 in IR7) is plotted versus time. The dip in the cleaning inefficiency shows the successful test of the tight settings for collimators. The average cleaning inefficiency was calculated to be 3.4×10^{-4}.

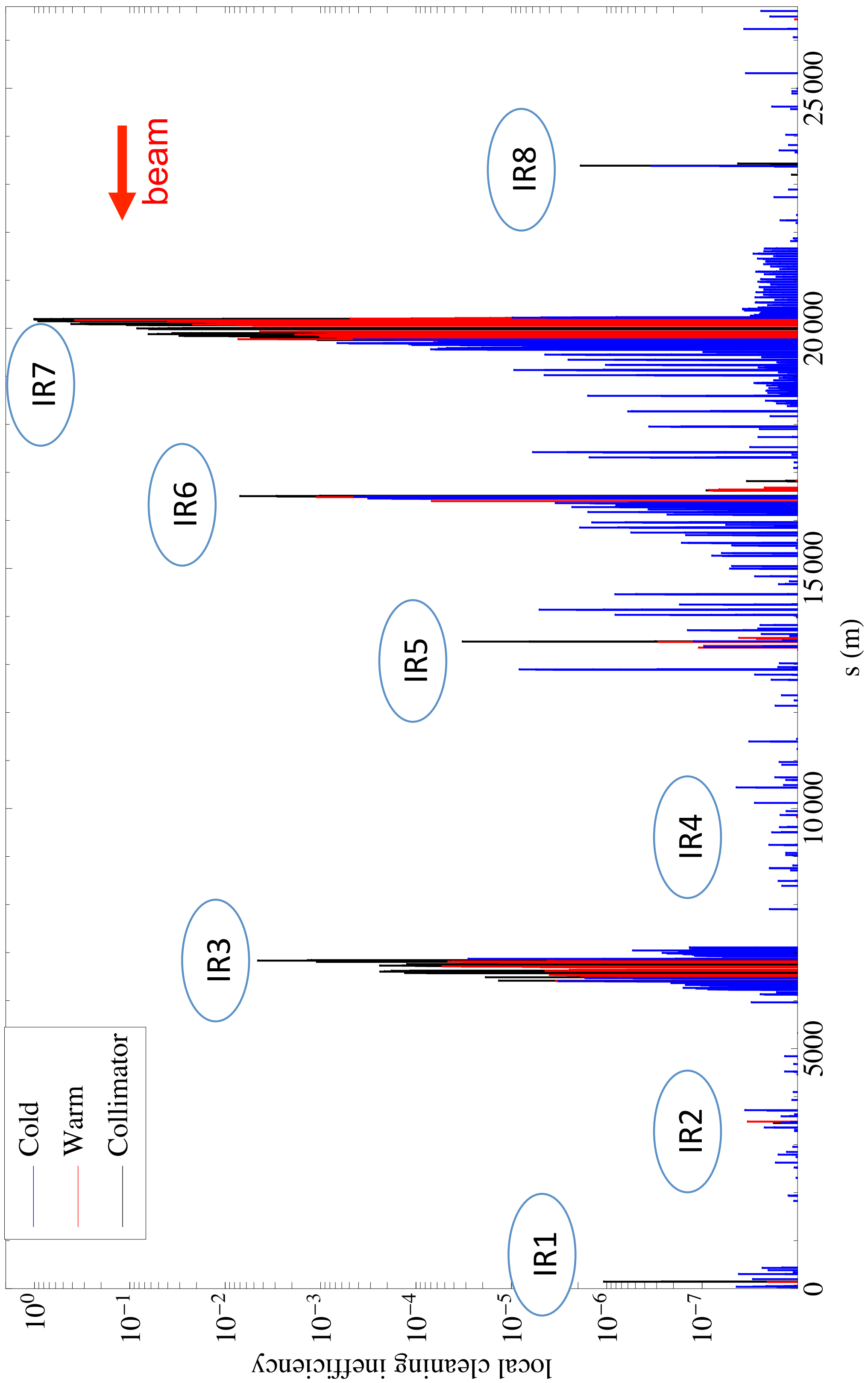

Fig. 6.1: Horizontal betatron loss map in beam 1. The beam is coming from the right. One can see the local cleaning inefficiency at each point of the LHC. The color-labeling shows the collimators (black), the warm region (red) and the cold regions (blue). The highest loss occurs on the vertical primary collimator in IR7. Other high losses can be found in IR6 and IR3.

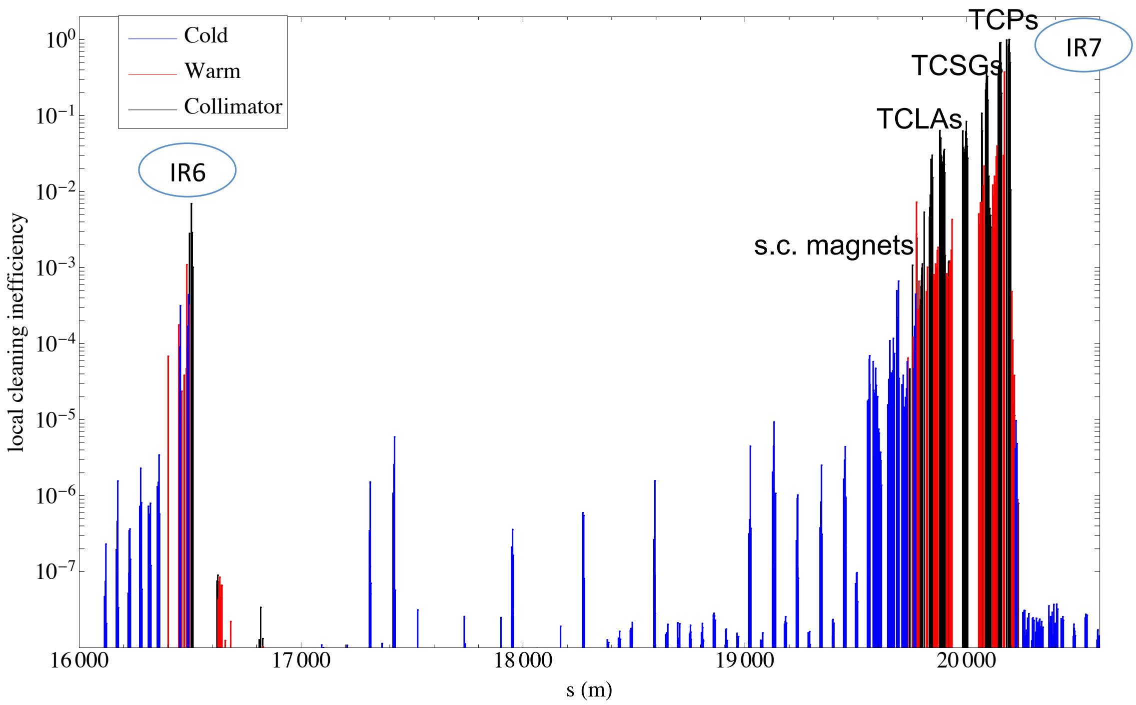

Fig. 6.2: Zoom in IR7. The hierarchy of the LHC collimation system can be seen.

6.2 Calibration factor for losses at collimators and sc magnets

It is of high interest to know how many particles are lost around the machine. The BLMs give the local distribution of the losses, while the total number of lost particles can be obtained from the Fast Beam Current Transformer (FBCT) signal. The BLMs are ionization chambers and the signals are in units of Gy/s. The beam intensity from the FBCTs is given in number of protons.

A calibration factor is necessary to calibrate the BLM signal to the particle loss rate achieved from the FBCT signal. With this method one can evaluate a local loss rate. The procedure to get this calibration factor is described in the following part.

In the first step one has to extract the signals of the FBCTs (S_{FBCT}) and the signals of the BLMs (S_{BLM}) from the database, which are available with frequency of 1 Hz. The number of lost protons within one second (measured $i+1$ minus measured i) is calculated as

$$\Delta S^i_{FBCT} = S^i_{FBCT} - S^{i+1}_{FBCT}, \tag{6.2}$$

which represents a particle loss rate for the full LHC. To reduce the noise this signal is averaged over 240 second and the loss rate R in second i is achieved as

$$R^i = \frac{1}{241} \sum_{i-120}^{i+120} \Delta S^i_{FBCT} \tag{6.3}$$

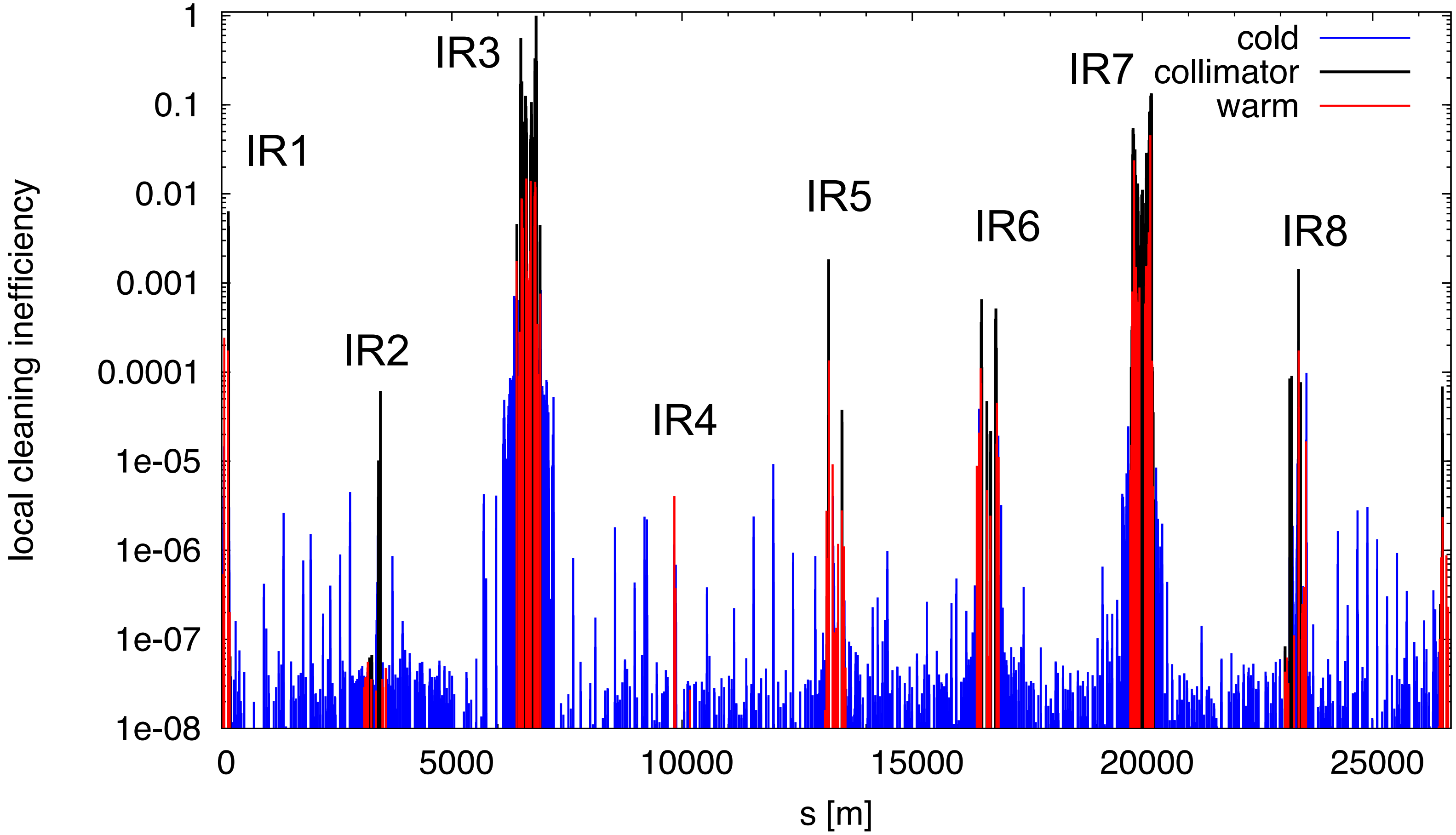

Fig. 6.3: Loss map with positive off momentum particles in beam 1 and beam 2. The highest losses occur at the primary collimators in the off-momentum cleaning insertion in IR3.

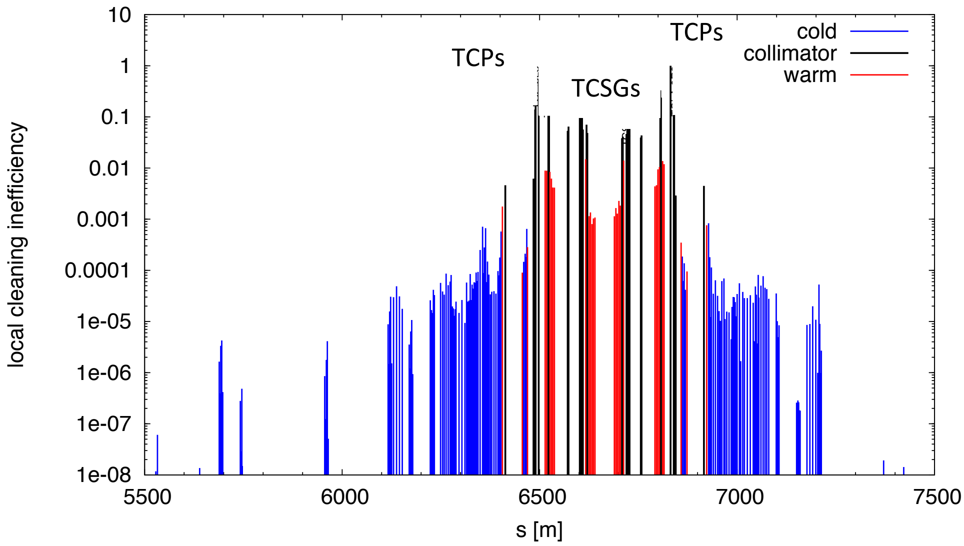

Fig. 6.4: Zoom in the off-momentum cleaning insertion in IR3.

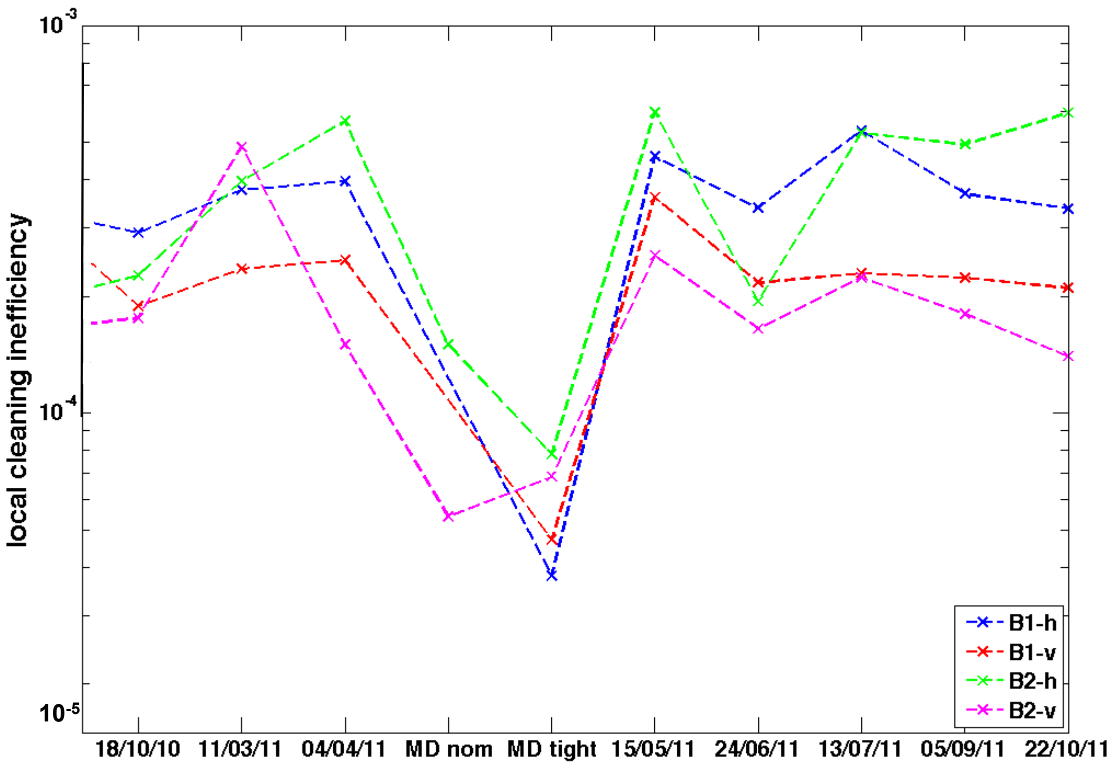

Fig. 6.5: Cleaning inefficiency versus time during the run in 2011. [30]

To identify the steady-state time (constant loss rate) of the signal and exclude loss peaks due to van der Meer scans, wirescans, UFOs, beam dumps, etc, it is useful to plot the BLM signal versus time.

The calibration factor is calculated as

$$f^i_{calib} = \frac{R^i}{S_{BLM}}. \tag{6.4}$$

The calibration factor for one fill is calculated by determining the average calibration factor $\overline{f^i_{calib}}$. The instantaneous loss rate at the primary collimator is then

$$R_{coll}\,[p/s] = \overline{f^i_{calib}}\,[p/Gy]\;\cdot\;S_{BLM}\,[Gy/s]. \tag{6.5}$$

To evaluate the loss rate at a magnet one has to scale the losses at the primary collimator by using the measured local cleaning inefficiency and assuming no changes in the BLM response (BLM response = 1):

$$R_{loss}(s) = R_{coll}\;\cdot\;\eta_{c,local}. \tag{6.6}$$

Note, that for the evaluation of the calibration factor a few assumptions were made, i.e. that the main fraction of lost particles impact at the primary collimators in IR7. Also the luminosity induced burn off was neglected, which becomes more important during the intensity increase. If more information was available (the BLM losses at all IRs) then f_{calib} would be calculated as:

$$f_{calib} = \frac{R_i}{S^{IR7}_{BLM} + S^{IR3}_{BLM} + S^{IR1}_{BLM} + S^{IR2}_{BLM} + S^{IR5}_{BLM} + S^{IR8}_{BLM}} \tag{6.7}$$

The calibration factor evaluated in this master thesis only takes into account S^{IR7}_{BLM} and f_{calib} is therefore overestimated.

6.3 Loss maps in Lost Power

The calibration factor also allows to evaluate the lost power. With this method one can determine the power impact at each point of the ring and compare this value to the quench limit. One has:

$$S_{BLM}[Gy/s]\cdot f_{calib}[p/Gy] = R_{coll}[p/s] \tag{6.8}$$

$$R_{coll}[p/s]\cdot E[eV/p] = R_{coll}[eV/s] \tag{6.9}$$

$$R_{coll}[eV/s]\cdot e[C] = R_{coll}[J/s] \tag{6.10}$$

$$R_{coll}[J/s] = R_{coll}[W] \tag{6.11}$$

with the particle momentum E and the electric charge e. As mentioned before one has to scale the achieved values for the lost power at the primary collimator with the local cleaning inefficiency to get the lost power around the ring:

$$R_{loss}(s) = R_{coll}\cdot\eta_{c,local}. \tag{6.12}$$

Tab. 6.1: Power impact in Watt for a selection of collimators and for the most affected magnets.

Collimator	TCP IR7	TCDQ in IR6	TCP in IR3	Q8L7	Q11L7
Power impact [Watt]	505000	2100	1900	338	40

Figure 11.1 shows the loss map from Figure 6.1 in terms of lost power versus s-position. Figure 6.7 shows a zoom of this in IR7.

For this loss map the highest loss was achieved at the vertical primary collimator in IR7 with a lost power of 505 kW over 1 second, this corresponds to 9.1 $\times 10^{11}$ lost protons per second. This loss map was used to demonstrate the design loss rate for the LHC of 500 kW on a primary collimator [32, 33]. A sample of collimators and the power impact during the performed loss map can be found in Table 6.3.

The losses in the cold regions are most important. They should be low enough to avoid quenches in the superconducting magnets. To evaluate the maximum cleaning inefficiency one has to look at the magnet with the highest losses. The highest losses in the cold region occur in the quadrupole magnet Q8 in the dispersion suppressor downstream of IR7. The peak power loss in the Q8 was 335 Watt. This value corresponds to a local cleaning inefficiency of 6.7 $\times 10^{-4}$ and a peak loss of 505 kWatt at the primary collimator.

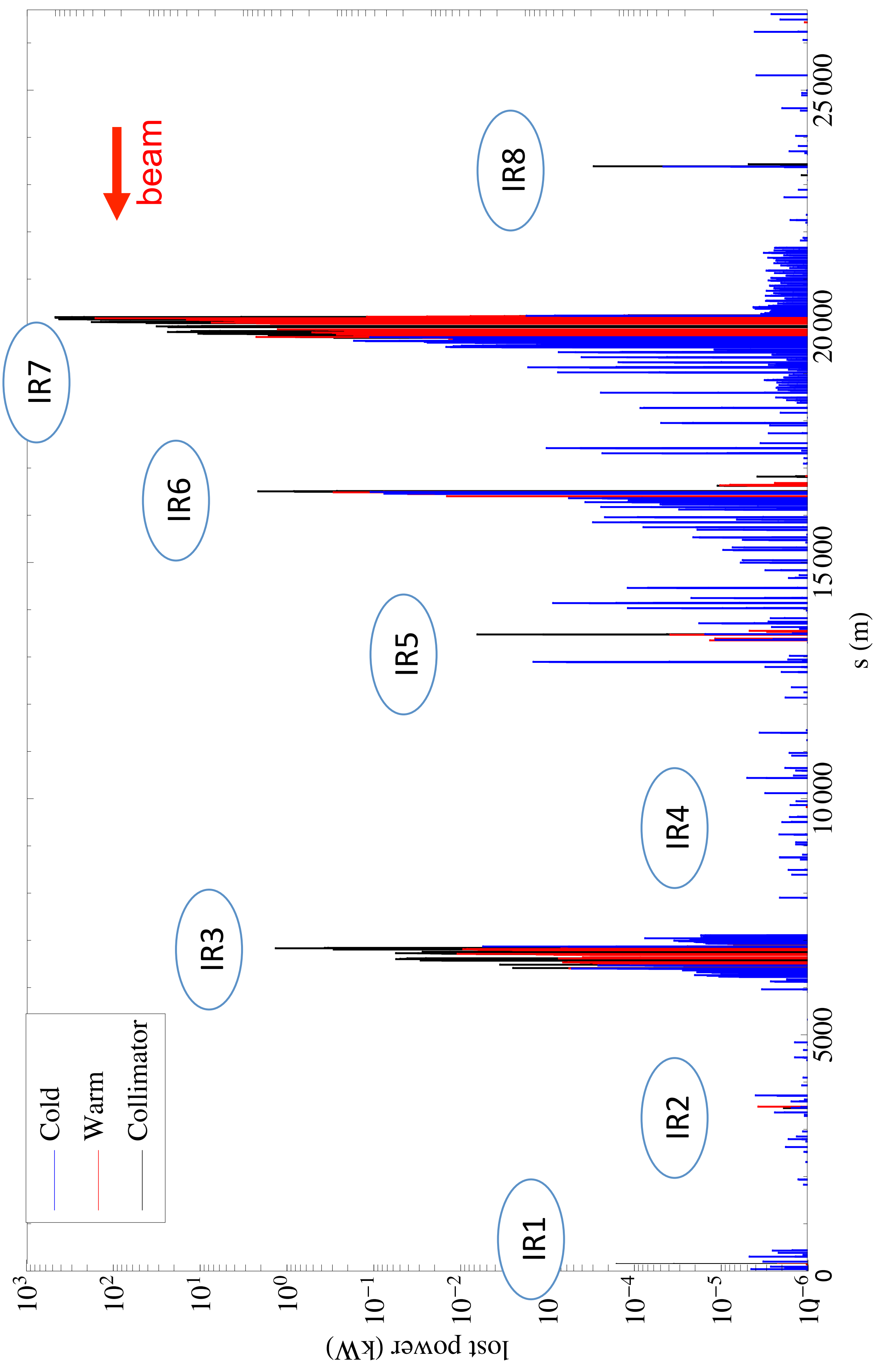

Fig. 6.6: Betatron loss map in the vertical plane in beam 2. The highest losses appear in IR7. The achieved peak loss power was 505 kW.

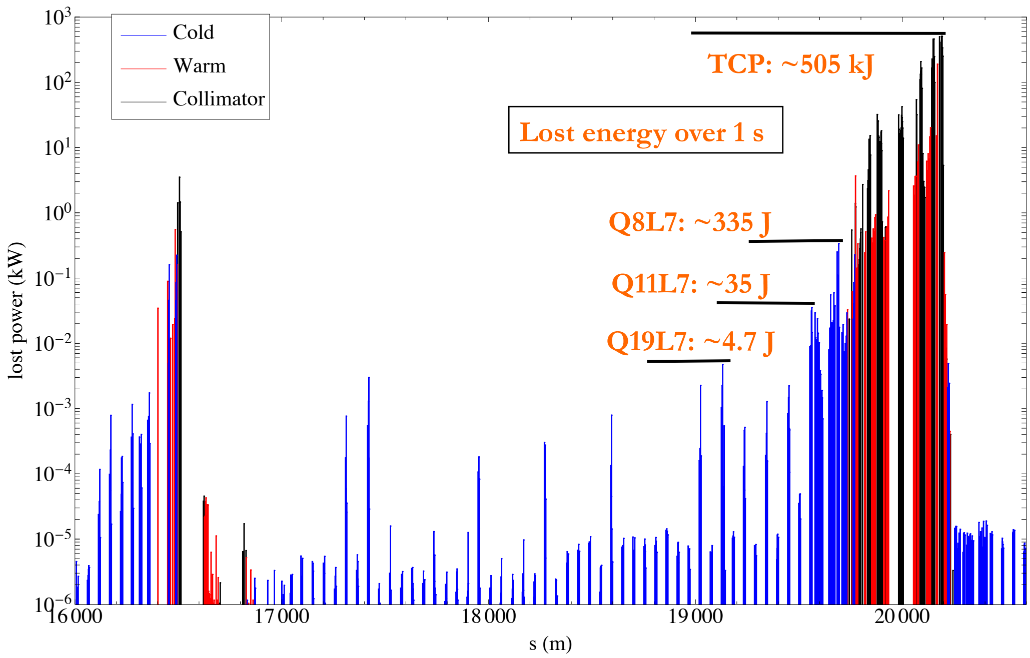

Fig. 6.7: Zoom in IR7 with the highest loss on the primary collimator (505 kW). Downstream one can see the hierarchy of the collimators and the losses at the quadrupole magnet after the cleaning insertion. The highest power impact occurs at the magnet Q8 with a value of 335 Watt.

7. BEAM SCRAPINGS WITH COLLIMATORS

Assuming stable beams conditions and excluding failure cases, the lost particles at the collimators are from the beam halo. To evaluate realistic particle distributions in the transverse plane of the beam one has to measure the particle density in the halo. This is performed with so-called halo scrapings. Within this chapter the halo scrapings will be introduced. The measurement procedure will be explained in detail. Also the results of different scrapings are presented and discussed.

7.1 Why Halo Scrapings?

Understanding the population and the shape of the beam halo is important to predict possible intensity limitations for collimation at 7 TeV. Therefore the population of the beam halo has been measured in the horizontal, vertical and skew planes, using the primary collimators of the LHC collimation system. The cleaning of the beam halo is the main purpose of this system, where the so-called primary collimators define the smallest aperture in the LHC. During physics operation at 3.5 TeV the lowest beam lifetimes and therefore the highest losses at primary collimators appear when the two LHC beams are brought into collision. As this could become an intensity limit for the LHC at 7 TeV it is important to measure the population and shape of the beam halo. From the beam intensity profile during the scraping it is possible to calculate the particle population at each position of the collimator

7.2 Measurement Procedure

Primary collimators in IR7 were used for the scraping measurements, as they are the most robust collimators. During a scraping one of the two collimator jaws was moved into the beam to scrape away particles of the halo.
In the LHC collimation system there are primary collimators in three planes, horizontal, vertical and the skew planes, which are used for scraping. Thus, for the first time scraping was performed in the skew plane.

During scraping one jaw is moved into the beam leading to scattering and absorption of intercepted particles. Due to phase-space mixing the jaw the limits the beam distribution on both sides of the phase space.

Two types of scraping have been performed, the so-called fast scraping and the step wise scraping.
In both cases the collimator jaw is moving with a speed of 2 mm/s. During fast scraping the jaw is moved with constant speed into the beam until the beam is fully scraped away. During step wise scraping the jaw is moved in steps of 5, 20, 40, 60 or

80 μm, with 5 μm being the smallest possible step size. For the step wise scraping the time interval between two steps is an important variable, which has a significant influence on the measurement results. Within this interval one can observe the so-called beam loss temporal tails, which can be explained by the exponential decay of the beam loss. Considering these effects and the limited MD time, the time interval was normally set to $\Delta t = 4s$.

Scrapings in 2011 were performed at injection energy of 450 GeV and at top energy of 3.5 TeV. Scrapings at 3.5 TeV could only be performed as so-called end-of-fill experiment. I.e. they were performed at the end of a physics fill with full beam intensity. The beams were then dumped by the BLMs, when the losses reached the dump limits. Only the tails could therefore be scraped at 3.5 TeV, not the core.

Scrapings at 3.5 TeV give a direct access to the beam distribution at top energy and in collision. These types of scraping are clearly limited, as they will cause high losses in and downstream of the collimation regions. As the BLM dump limits must be always active in these conditions, the beams can only be partly scraped away, before the beams will be automatically dumped. Therefore the biggest part of scrapings were performed at 450 GeV with different intensities ($\approx$ 1.15 - 3.5e11 p) and, thus the full beam could be scraped without reaching the dump threshold of the BLMs. This is called full scraping. In addition scrapings at 450 GeV are more time efficient as the LHC can quickly be refilled after each scraping and no energy ramp is needed. This allows many scrapings in a relatively short time. In 2011 two dedicated MDs of each 4 h were used to perform scrapings with the LHC collimators.

7.3 Calibration factor for scrapings

To calculate the instantaneous particle losses at a primary collimator it was necessary to calibrate the beam intensity signals from the fast beam current transformers (FBCT) to the signals from the beam loss monitor S^i_{blm} on the corresponding collimator. Here a similar method as described in chapter 6.2 was applied.

Calibration factors were calculated for different running sums of the BLM signals. Running sums are different integration times for the BLM signals, which allow the analysis of losses with time scales from half a LHC turn (40 μs) up to 83.88 s. Table 7.3 lists the available BLM running sums and the corresponding number of LHC turns. In bold are the ones specially used for this thesis. All BLM signals are published and logged with a frequency of 1 Hz.

Note, that during the beam scrapings the loss is short compared to the integration time. Therefore the BLM signals S_{BLM} have to be divided by the running sum to get a real signal for the particle loss, which is not diluted by the integration over a time interval. For example in RS09

$$S^{loss}_{BLM} = \frac{1}{1.3} S_{BLM}. \tag{7.1}$$

For the calibration factor calculated for physics fills, where we assume a constant loss rate, this is not necessary.

Tab. 7.1: Available BLM running sums in the LHC. The running sums mainly used for this thesis are marked in bold.

Running sum	time interval Δt	Number of LHC turns	Definition
01	40 μs	0.5	peak loss
02	80 μs	1	peak loss
03	320 μs	4	peak loss
04	640 μs	8	peak loss
05	2.56 ms	32	peak loss
06	**10.24 ms**	**128**	peak loss
07	81.92 ms	1024	peak loss
08	655.36 ms	8192	peak loss
09	**1.3 s**	**14600**	integrated loss
10	5.24 s	58850	integrated loss
11	20.97 s	235396	integrated loss
12	83.88 s	941584	integrated loss

Figure 7.1 shows a plot of the loss rate versus the BLM signal for RS 09 (blue) and RS06 (red). The calibration factors were calculated as linear fit (solid lines) to the measured data. They were found as 9.9×10^{11} p/Gy for RS09 and 3.4×10^{11} p/Gy for RS06.

An overview of the calibration factors f^i_{calib} for the different slow scrapings during the Machine Development in July 2011 is shown in Table 7.2. It summarizes the calculated calibration factors f^i_{calib} for the slow scrapings with the IR7 primary collimators. This was measured in July 2011 for RS09 at the BLM directly on the collimator which was used for the scraping.

Tab. 7.2: Summary of the calculated calibration factors f^i_{calib} for the slow scrapings with the IR7 primary collimators as measured in July 2011 for RS09.

Scraping	f^i_{calib} [p/Gy] B1	f^i_{calib} [p/Gy] B2
slow vertical (TCP.D)	1.20×10^{12}	1.13×10^{12}
slow horizontal (TCP.C)	1.25×10^{12}	1.26×10^{12}
slow skew (TCP.B)	1.94×10^{12}	1.75×10^{12}

The average calibration factor achieved from scrapings and physics fills for the BLM at the horizontal collimator in IR7 (TCP.C) was calculated as 1.2×10^{12} p/Gy $\pm$ 2.08×10^{11} p/Gy for RS09 and 5.2×10^{11} p/Gy $\pm$ 3.87×10^{11} p/Gy for RS06.

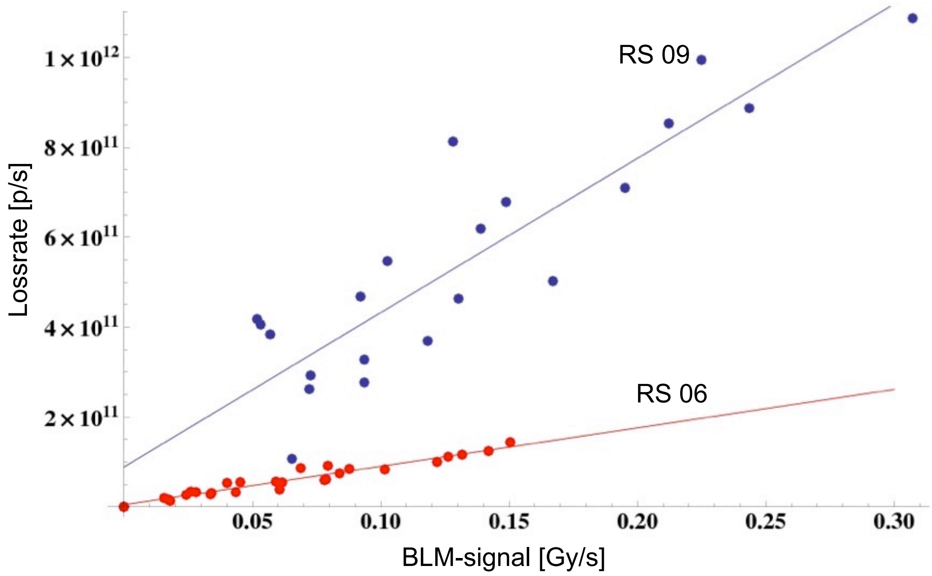

Fig. 7.1: Plot of the loss rate versus the BLM signal for RS09 (blue) and RS06 (red). The calibration factors were achieved from a linear fit of the data. They were calculated as 9.9×10^{11} p/Gy (RS09) and 3.4×10^{11} p/Gy (RS06).

8. BEAM SHAPE

Knowing the real shape of the beam in the LHC is important to identify limitations of future machine upgrades (e.g. crab cavities) with respect to machine protection requirements. To measure the real beam shape beam scrapings were performed with collimators during machine development (MD) studies and as end of fill studies. Within this chapter the results of the full scraping, the comparison to end-of-fill studies and the different fit types are presented and discussed.

8.1 Evaluation of lost intensity during scrapings

The instantaneous particle loss rate at collimator i can be calculated with the calibration factor and the BLM signal as

$$R_i(t) = f^i_{calib} S^i_{blm}(t). \tag{8.1}$$

With one step every 4 seconds and the publishing frequency of the BLM signals of 1 Hz the lost intensity at each collimator jaw position u is given as

$$I_L(u) = \sum_{j=1}^{4} \left(R_i(t_{u,j}) \cdot 1s\right). \tag{8.2}$$

where $t_{u,j}$ is the time when the collimator jaw is on position u.

The remaining intensity in the beam at each collimator jaw position u can then be written as

$$I(u) = \sum_{u}^{u_{end}} I_L(u) = \sum_{u}^{u_{end}} \sum_{j=1}^{4} \left(R_i(t_{u,j}) \cdot 1s\right), \tag{8.3}$$

with $I(u_{end}) = 0$.

The total intensity is given by

$$I_{total} = \sum_{u_{start}}^{u_{end}} I_L(u), \tag{8.4}$$

with the starting position of the collimator jaw u_{start}.

The normalized and integrated lost intensity at the collimator jaw position u can be calculated as

$$I_{tot,lost}(u) = \sum_{u_{start}}^{u} I_L(u)/I_{total}. \tag{8.5}$$

8.2 Single gaussian fit

Assuming that a particle beam has a gaussian shape one can fit the results of a full beam scraping with gaussian curve

$$I(u) = I\left(1 - exp\left[\frac{-(u-\mu)^2}{\sqrt{2}\sigma^2}\right]\right), \tag{8.6}$$

with the measured intensity I, the collimator position u, the beam offset μ and the beam size σ. Figure 8.1 shows the measured beam shape for a step wise scraping at 450 GeV. The step size of the collimator jaw movement was 10 μm with a interval of 4 s. It is clearly visible that there is a significant disagreement between the measured and the fitted curve above 0.5 σ. The measured tail population is higher than expected from a gaussian fit.
The difference to a gaussian distribution, as expected from electron-machines, can be explained by the much smaller synchrotronradiation-damping.
The fit coefficient μ gives the position where the beam centre is expected. For the fit this coefficient was evaluated with a fit error of 0.1 mm. Compared to a collimation setup, where the jaws were centred around the beam, the variation of the beam offset was found with an agreement better than 210 μm in Beam 2 and 350 μm in Beam 1. The emittance of the beam was calculated from the fitted beam size with

$$\epsilon = \frac{\sigma^2}{\beta}. \tag{8.7}$$

This was compared to the emittance from wire scanner measurements. A maximum difference of 1.5 nm was found.

8.3 Double gaussian fit

To improve the agreement between fit and data the single gaussian was extended to a double gaussian

$$I(u) = I_1\left(1 - exp\left[\frac{-(u-\mu)^2}{\sqrt{2}\sigma_1^2}\right]\right) + I_2\left(1 - exp\left[\frac{-(u-\mu)^2}{\sqrt{2}\sigma_2^2}\right]\right). \tag{8.8}$$

Here the fit coefficients are the intensities I_1 and I_2 for the two gaussians, the beam offset μ and the two sigmas σ_1 and σ_2. Figure 8.2 shows the measured beam data from Figure 8.1 with the fit of a double gaussian. The fit agrees well with the data up to $x \approx 5\sigma$. Above this value the measured halo population cannot be sufficiently fitted with the model.

These results also hold for scraping data obtained in other planes.

8.4 Scrapings at 3.5 TeV

The scrapings at 3.5 TeV were performed as end of fill (EOF) experiments. As mentioned earlier only a few steps of the collimator jaw were feasible before the

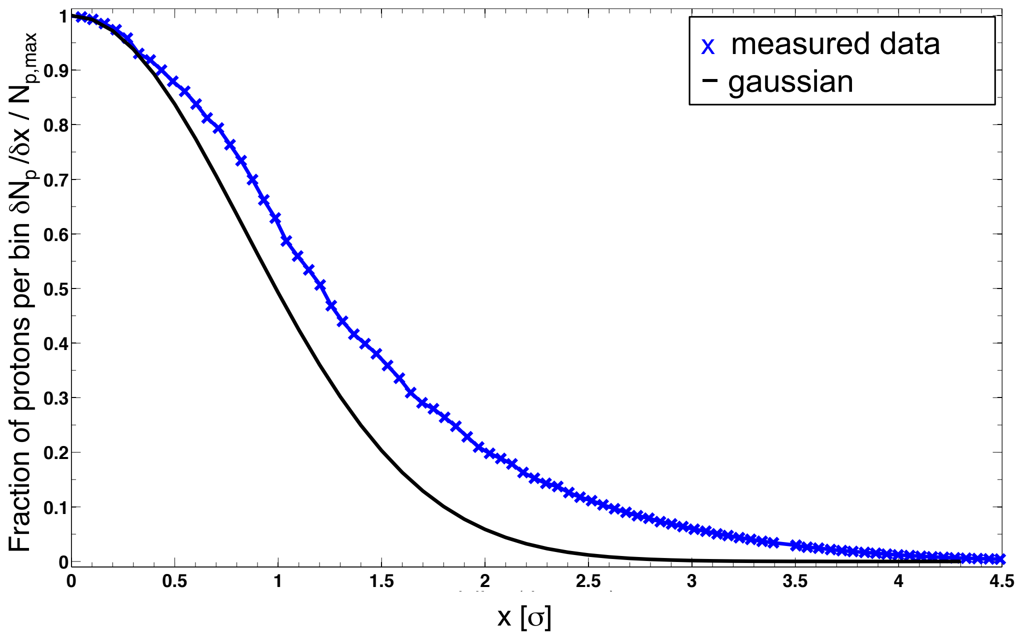

Fig. 8.1: Horizontal beam shape at 450 GeV compared to a gaussian curve. The beam shape was evaluated with a step wise scraping with the horizontal primary collimator in IR7. With a step size of 10 μm and a repetition rate of 4 s.

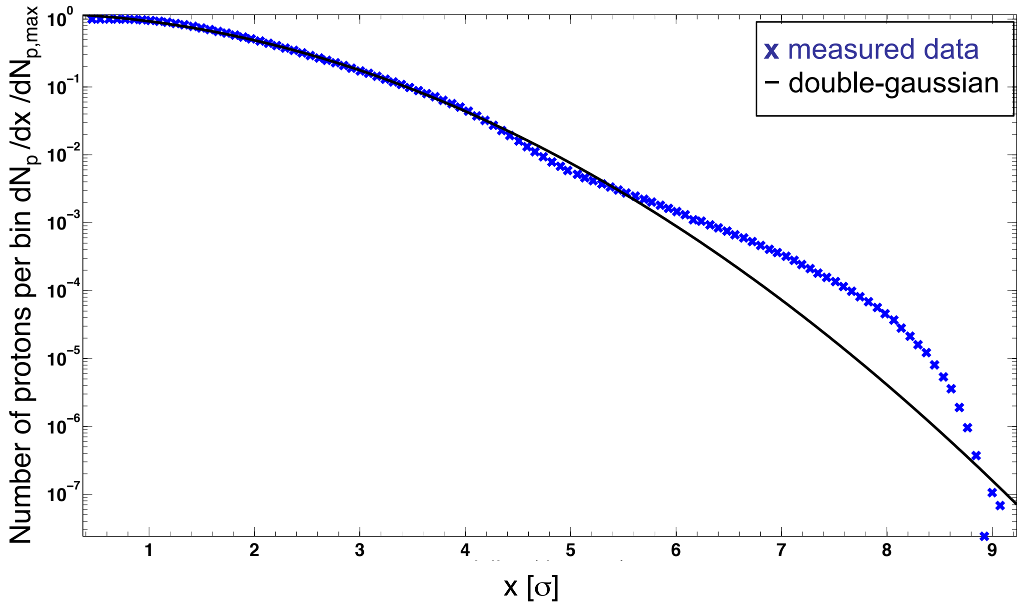

Fig. 8.2: Horizontal beam shape at 450 GeV with the fit curve of double gaussian.

losses reached the BLM dump threshold and therefore caused a beam dump. 6 EOF studies were performed in 2011. Figure 8.3 compares an EOF scraping after 8 hours of collision with 912 bunches (I ≈ 1e14 p) and a scraping performed at a special fill for an experiment with the TOTEM detectors (I ≈ 2.5e11 p). For reference a gaussian is also depicted. A comparison of the measured beam population at 3.5 TeV and 450 GeV is shown in Figure 11.4. For reference a gaussian is also depicted.

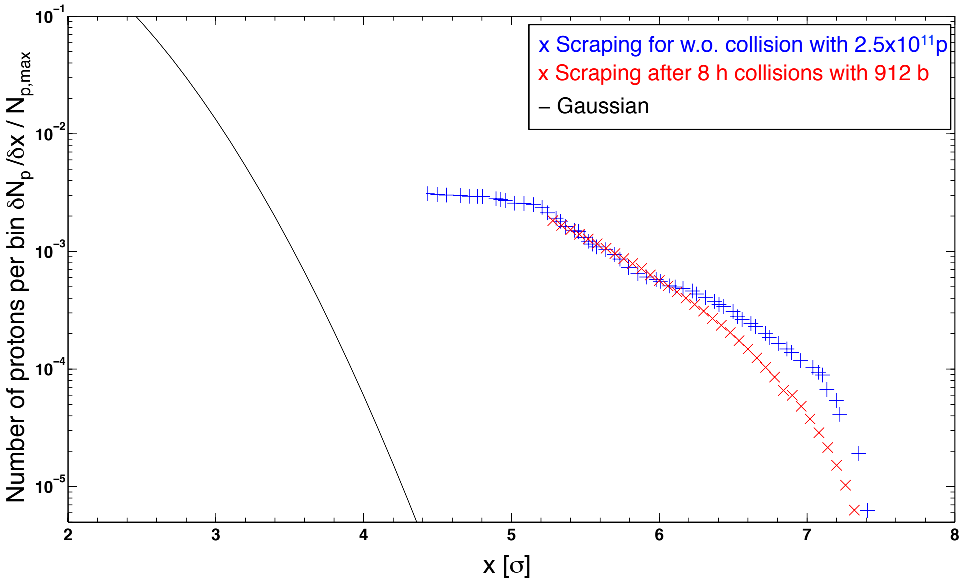

Fig. 8.3: Horizontal beam shape for two different scrapings at top energy. After 8 hours of colliding beams with 912 bunches (red) and during the preparation for an experiment with the TOTEM detectors (blue). For comparison a gaussian curve is depicted.

The shape of the beam tail at 3.5 TeV is comparable to the one found at 450 GeV until $x \approx 5.2\sigma$ when the beam was dumped. The tail population at 3.5 TeV is a bit lower for large amplitudes. For this measurement a step size of 20 μm was taken for step wise scraping at 450 GeV with a time interval of 4 s. At 3.5 TeV the scraping was performed with a step size of 10 μm and also 4 s as time interval.

8.5 *Tail population*

In Figure 11.3 the comparison of horizontal, vertical and skew halo population at 450 GeV with a step size of 10 μm and an interval between the steps of 4 s (scaled to nominal intensity of 3.0×10^{14}p) is depicted. Note that a beam profile in the skew plane was measured for the first time. Figure 8.6 shows the vertical beam population at 450 GeV scaled to nominal intensity 3.0×10^{14} p. The dashed line indicates 4 σ. 1.9 % of the total intensity were found above this value.

Table 8.1 summarizes the fraction of the beam population above 4 σ_{meas} found during the scrapings in the three planes at 450 GeV. The measurements were performed with 10 μm step size and an interval of 4 s. The number of protons, stored

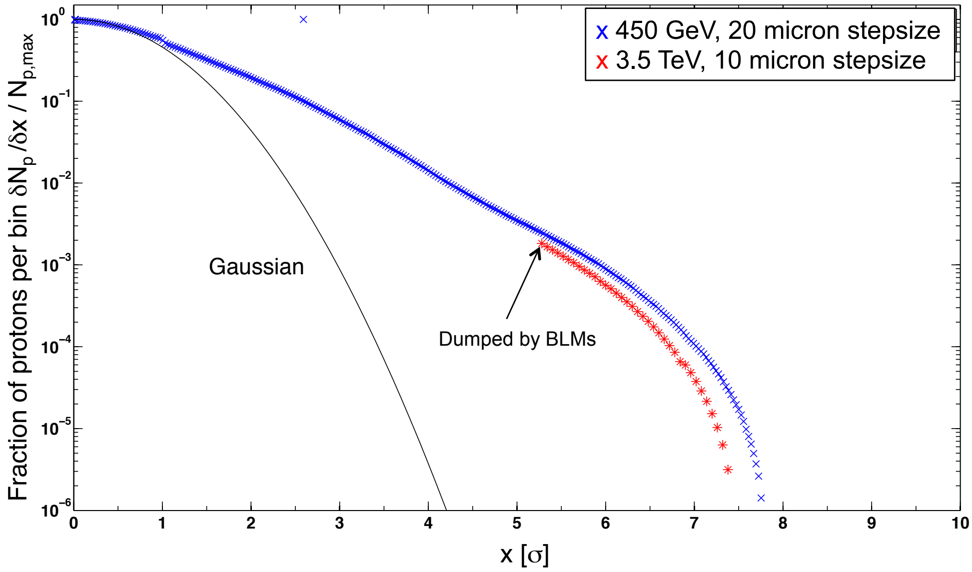

Fig. 8.4: Comparison of the beam shape in the horizontal plane at 450 GeV (blue) and 3.5 TeV (red). For reference a gaussian (black) is also depicted.

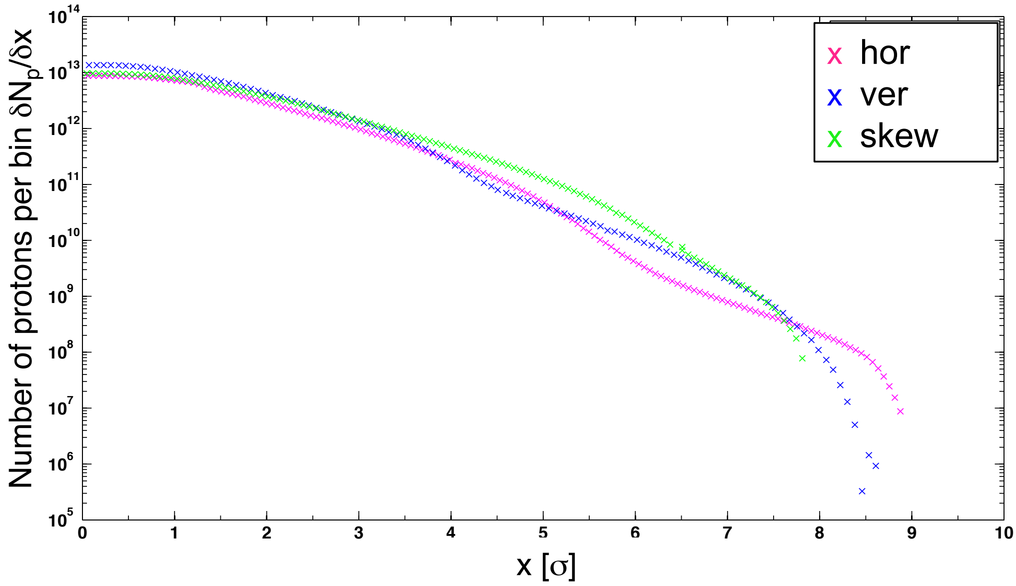

Fig. 8.5: The beam shape of the LHC beam in all planes. Horizontal plane (red), vertical plane (blue) and the skew plane (green). The scrapings were all performed with a step size of 20 μm and a time interval of 4 s at 450 GeV.

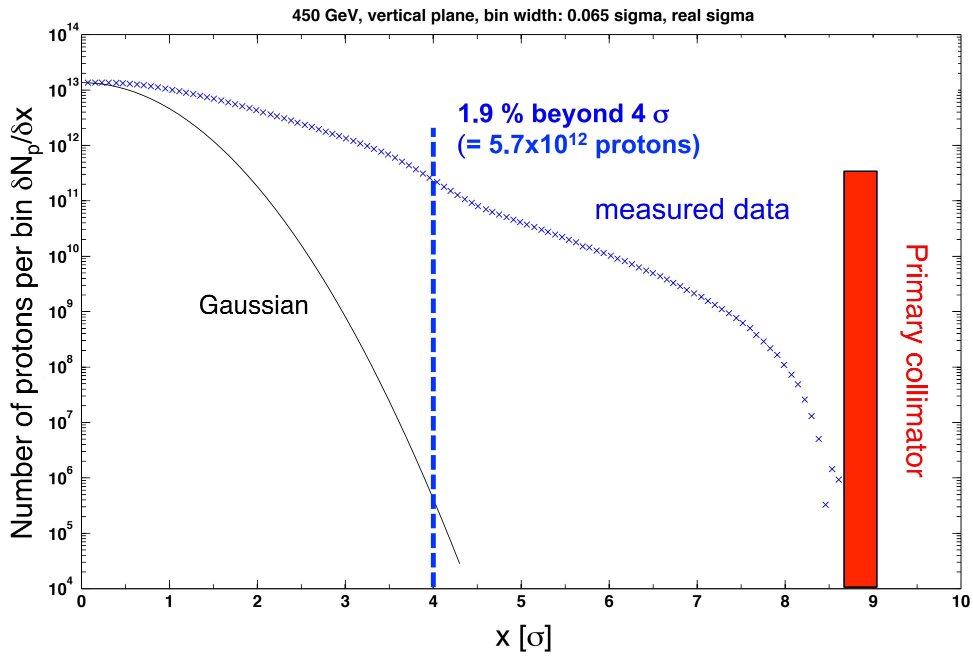

Fig. 8.6: The beam shape in the vertical plane. Scaled to design intensity. Measured with step wise scraping at 450 GeV with a step size of 20 μm and a time interval of 4s. The dashed line shows the number of protons above 4 measured σ.

beam energy and TNT equivalent was calculated for a nominal intensity of 3×10^{14} p.

8.6 Comparison of fast and slow scrapings

The comparison of the measured beam population during fast and slow scraping in the vertical planes of B1 is shown in Figure 8.7 . It can be clearly seen that the width of the beam distributions measured during the fast scraping is $\sim$ 70% of the width measured during the slow scrapings. This behaviour can possibly be explained from the previously observed temporal loss tails during beam scrapings with collimators.

Tab. 8.1: Measured tail population above 4 σ_{meas}. The number of protons, the stored beam energy in the beam tails and the corresponding value in kg TNT are scaled to a total beam intensity of 3×10^{14} p.

Plane	Horizontal	Vertical	Skew
Fraction of beam intensity above 4 σ	2.7 %	1.9 %	3.6 %
Number of protons (scaled to design beam intensity)	8.1×10^{12}	5.7×10^{12}	10.8×10^{12}
Energy stored in beam tails at 7 TeV and design beam intensity [MJ]	9.8	6.9	13
Corresponding value in kg TNT	2.2	1.5	2.8

These temporal tails were also observed during slow beam scraping. Figure 8.9 shows a comparison between the lost particles during each step of the collimator movement, $I_L(u)$, which are summed over the 4 seconds of the step, and the lost particles per second, $R_i(t)$, during slow scraping with the vertical primary collimator. Figure 8.10 shows the ratio of these two measures. It can clearly be seen that the losses described by $R_i(t)$ per 1 s are about $\sim 70\%$ of I_L. The physical processes, which cause these temporal tails are currently under investigation. During a fast scraping these temporal tails are not taken into account. This causes a smaller measured width of the measured beam distribution compared to slow scraping. The same occurs in the measurements of Beam 2.

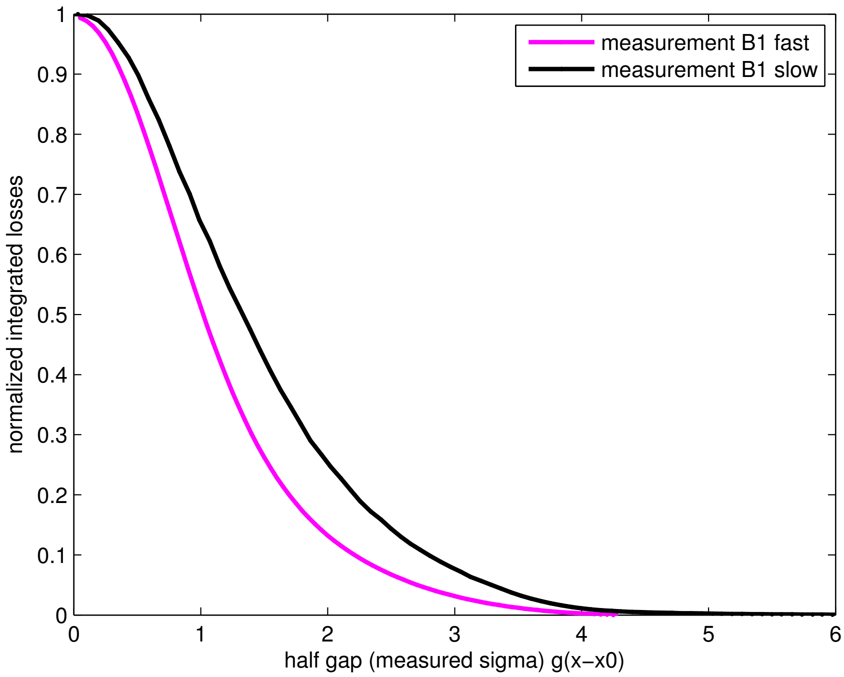

Fig. 8.7: Comparison of normalized integrated lost beam intensity, $I_{tot,lost}(u)/I_{total}$, versus jaw position in units of measured beam sigma, σ_{meas}, during step wise (black) and fast (magenta) vertical scraping on B1. Note: $\sigma_{meas} = 0$ was assumed for the collimator jaw position $u_i = \mu_{i,0}$, with the fitted beam offset $\mu_{i,0}$ for scraping i.

Figure 8.8 shows the beam intensity during the MD performed in July. The filling with one bunch and then the slow loss of beam intensity during the step wise scraping can be seen. The scrapings were performed in the three planes. At the end of the MD a fast scraping in the vertical plane was performed and the beam intensity is going to zero within 2 s [34].

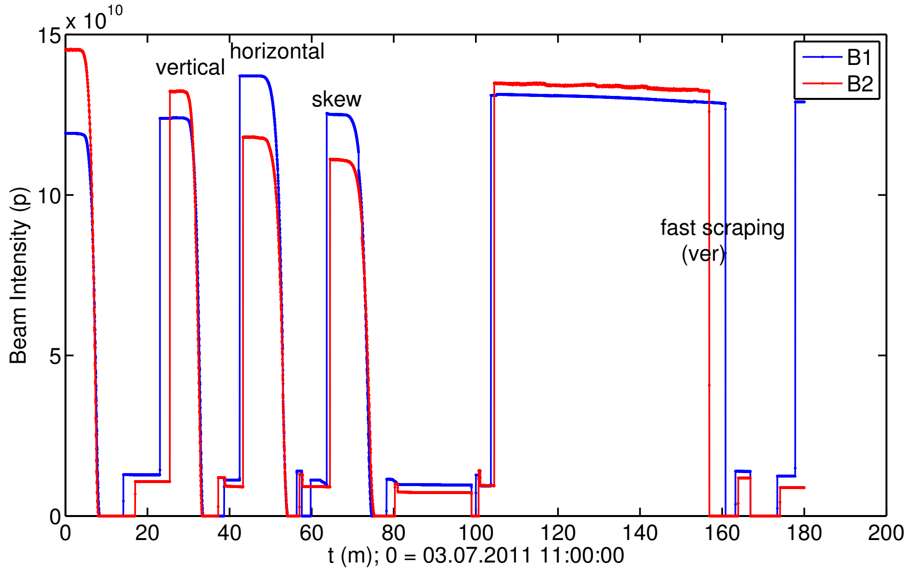

Fig. 8.8: Beam intensity of the two beams during the machine development in July 2011. One can nicely see the injection of the beams and then the scraping of the beams with a delay of 4 seconds (in the time between injection and scraping wirescans were performed to measure the emittance of the beams). Also the comparison of step wise and fast scraping can be seen here.

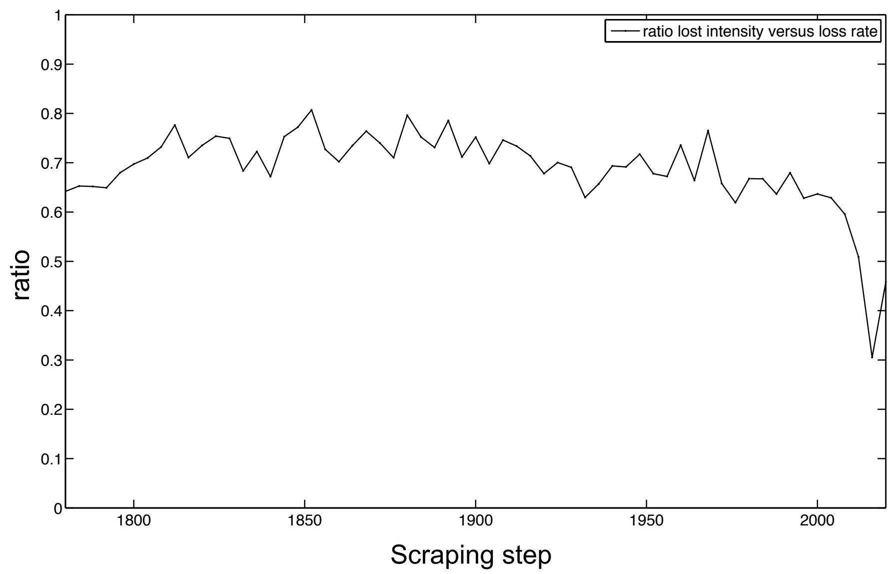

Fig. 8.9: Ratio of the lost intensity at each scraping step, $I_L(u)$, and the intensity lost in a second, $R_i(t)1s$, during a slow vertical scraping with the TCP.D6L7.B1.

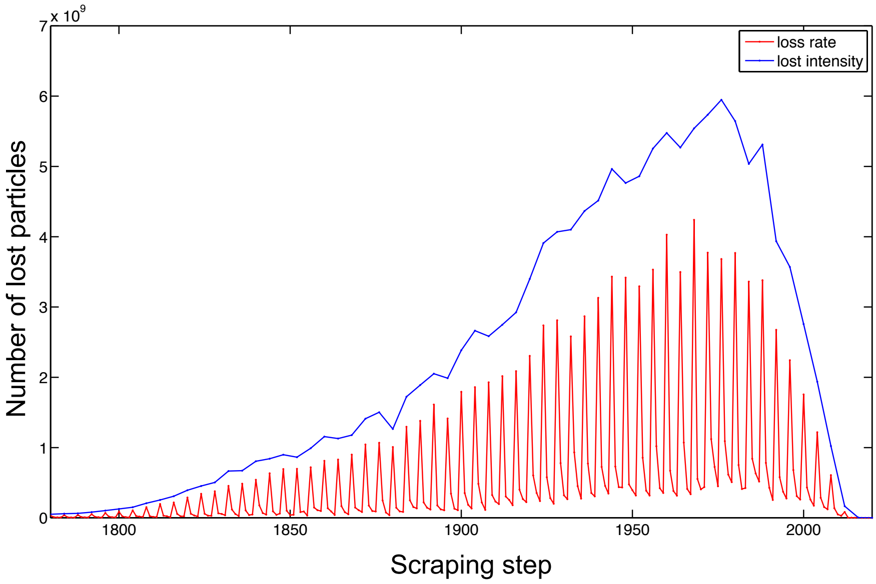

Fig. 8.10: Comparison of the lost intensity at each scraping step, $I_L(u)$, and the intensity lost in a second, $R_i(t)1s$, during a slow vertical scraping with the TCP.D6L7.B1.

9. INSTANTANEOUS LIFETIMES DURING PHYSICS RUNS

The instantaneous lifetime at collimators is an important measure to identify possible limitations in LHC collimation. Within this chapter, the lifetime evolution of the beams during a physics fill will be discussed. One can find the lifetimes for each part of a fill, like injection, ramp, squeeze and stable beams. The minimum lifetimes for the physics fills in 2011 are presented.

9.1 Instantaneous Lifetimes measured with the LHC Collimators

The minimum lifetime is important to evaluate possible performance limitations of the LHC in collimation. The maximum beam intensity $N_{i,max}$ is given by

$$N_{i,max} = \frac{\tau_{min}\, R_q\, L_{dil}}{\tilde{\eta}_c}\, c_{blm} \tag{9.1}$$

with the minimum beam lifetime τ_{min}, the quench limit R_q, the dilution length L_{dil}, the cleaning inefficiency $\tilde{\eta}_c$ and the BLM threshold factor c_{blm}. The BLM threshold factor was defined to guarantee safe machine operation and has a value of 1/3.

Figure 9.1 shows the BLM signals around the whole length of the LHC during a fill with 336 bunches at the beginning of the 2011 run. Note that the BLM signals are plotted in linear scale. Summing the losses in the different IRs, shows that $\sim$ 87 % of the losses appear in the betatron cleaning insertions IR7 and 2.5 % appear in the momentum cleaning. Thus, the dominating part of the losses is at the primary collimators in IR7. Therefore it is justified to calculate the instantaneous beam lifetime from the BLM signals at the IR7 primaries. Clearly, with increasing instantaneous luminosity the fraction of protons burned off in collisions will increase. This causes an underestimation of the instantaneous lifetime calculated from the losses at primary collimators. For the future the lifetime and loss rate should be corrected for the luminosity burnoff. This is not done within this thesis.

9.2 Proton Runs

Within this section a typical proton physics fill will be presented and discussed. Fill 2195 was used as an example. Table 9.1 summarizes the main parameters of this fill. The steps of the analysis are:

- Extraction of the intensity signal of the FBCTs and beam loss signals of the BLMs at the primary collimators in IR7.

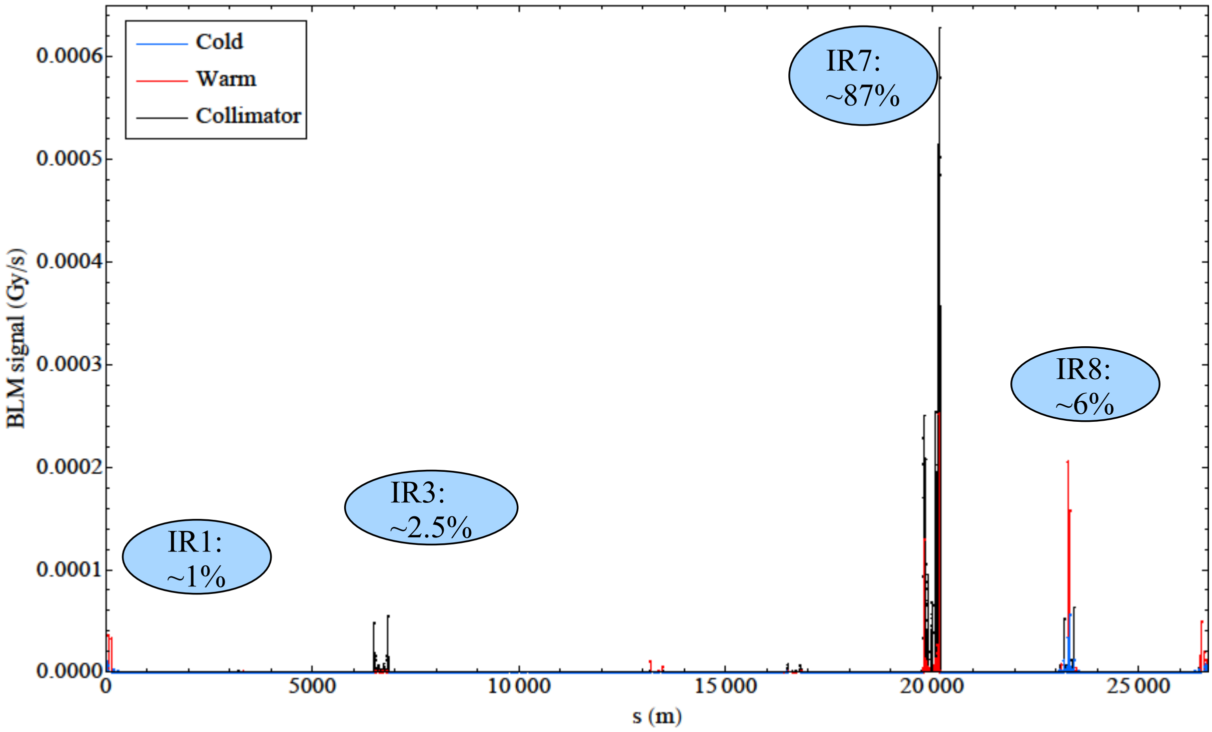

Fig. 9.1: Loss distribution around the LHC in linear scale. 87 % of the losses occur in IR7. This was calculated for physics operation with 336 bunches. The loss distribution changes for higher luminosity as the luminosity burn off induces losses around the IRs.

Tab. 9.1: Overview of parameters for fill 2195. [8]

Fill number	2195
Start Date	08.10.2012
Duration stable beams [h]	17:17
Energy [GeV]	3500
Number of bunches	1380
Maximum intensity [p]	1.79×10^{12}
Delivered luminosity from ATLAS [nb^{-1}]	114912.8
Delivered luminosity from CMS [nb^{-1}]	120134.7

- Achieving a calibration factor to translate the BLM signals into a particle loss rate at the collimator (see method in chapter 6.2).
- Calculation of the particle loss rate R_{coll} at the collimator.

From the loss rate one can derive the instantaneous beam lifetime τ as

$$\tau_{inst}(t) \approx \frac{N}{R_{coll}(t)} \tag{9.2}$$

with the beam intensity N and the instantaneous loss rate at the primary collimator $R_{coll}(t)$.

Figure 9.2 shows the beam intensity in both beams during fill 2195. During the 17 h of luminosity production the beam intensity slowly decreases.

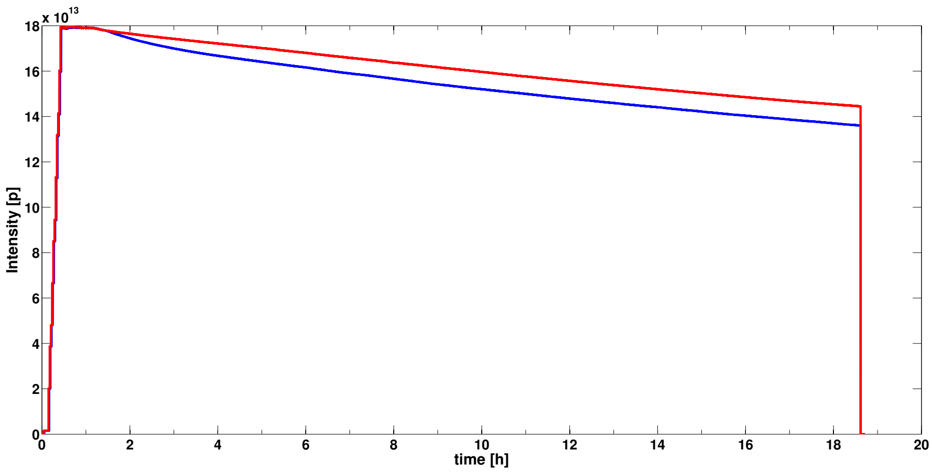

Fig. 9.2: The beam intensity of Beam 1 (blue) and Beam 2 (red) during fill 2195. One can see the increase of the intensity during the filling and then a slow decrease during luminosity production. Afterwards one can see the beam dump.

Figure 9.3 shows the BLM signal at the horizontal primary collimator in IR7 for B1. This BLM also sees showers from losses appearing from the vertical primary collimator that is installed a few meters upstream. The highest BLM signal can be found after the ramp, when the beams were brought into collision. The loss peaks marked in the plot, which appear during the fill are caused by the so-called UFOs, dust particles which fall through the beam and cause high losses.

The loss rate at the collimator can be seen in Figure 9.4. The instantaneous beam lifetime calculation with the help of Equation 8.2 is shown in Figure 9.5.

The average beam lifetime during stable beams was 100 hours. The minimum instantaneous lifetime during the whole fill was 14.8 h, when the beams where brought into collision ($t \approx 0.7h$). Figure 9.6 shows the instantaneous lifetime during the injection process, the energy ramp, flat top and squeeze energy of 3.5 TeV. The small dips during the injection are caused by the injection of bunch trains (0-0.2 h). The lifetime stays constant during the preparation of the ramp (0.2-0.32 h), which is

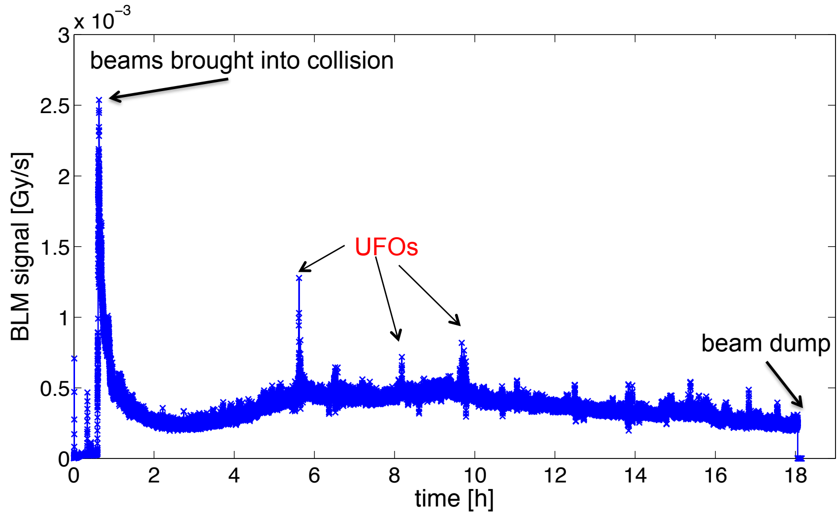

Fig. 9.3: Signal of the BLM at the horizontal TCP over the fill. The highest loss occurs, when the beams were brought into collision. Before that the losses were caused by ramp and squeeze. During stable beams UFOs were observed and after 17 h of colliding beams the beam was dumped.

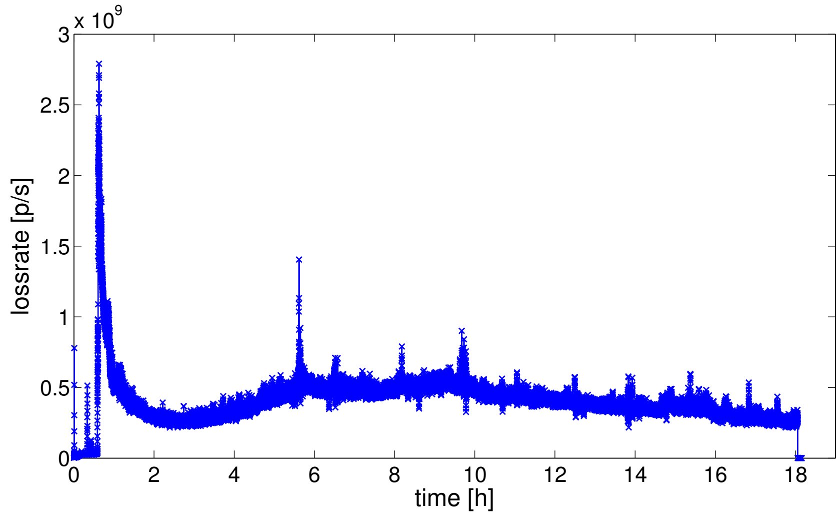

Fig. 9.4: Particle loss rate at the horizontal collimator during fill 2195, calculated from the BLM signal.

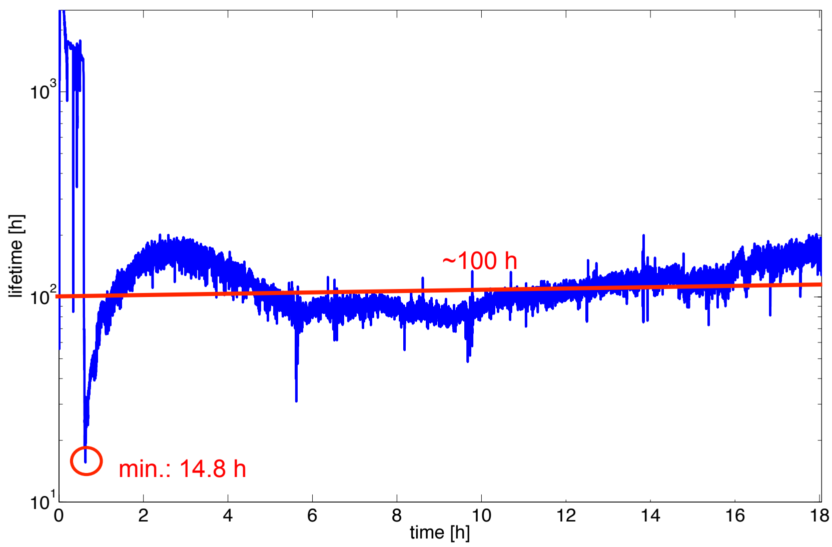

Fig. 9.5: Beam lifetime during fill 2195. The average lifetime during stable beams was 100 hours. The minimum instantaneous lifetime was 14.8 hours. This appeared when the beams were brought into collision.

followed by the ramp and the squeeze (0.32-0.57 h). During the ramp the collimator gaps are reduced following the adiabatic damping with beam energy.

Figure 9.7 shows a zoom into the part of the fill with the lowest lifetime of 14.8 h. This appear due to the reduction of the dynamic aperture when the two beams are brought into collision. The part of the halo outside the reduced dynamic aperture is then cleaned out by the primary collimators.
After this lifetime dip the losses slowly reduce and the lifetime stabilizes around 100 hours. With the decrease in intensity during the fill the lifetime slowly increases this is shown in Figure 9.8.

During the intensity increase in 2011 from 612 up to 1380 bunches 95 physics fills were analysed. Figure 11.2 shows the minimum lifetimes per fill for RS09 and RS06 and both beams. The conditions were:

- Time between start of adjust mode and beam dump.
- Collimation dependent lifetime.
- Losses at the vertical primary collimator in IR7.
- Intensity from 612 up to 1380 bunches.

Changes in intensity, β^* and tune are marked in the plot. The solid lines show the average beam lifetime for beam 1 and beam 2.

Tables 9.2 and 9.3 summarizes the results of the analysis. The minimum lifetime, the overall minimum lifetime and average values for changes in β^* and tune are shown.

Table 9.2 shows the average beam lifetime for Beam 1 and Beam 2 for RS09 and RS06 taking only the best 90 % of the analysed fills.

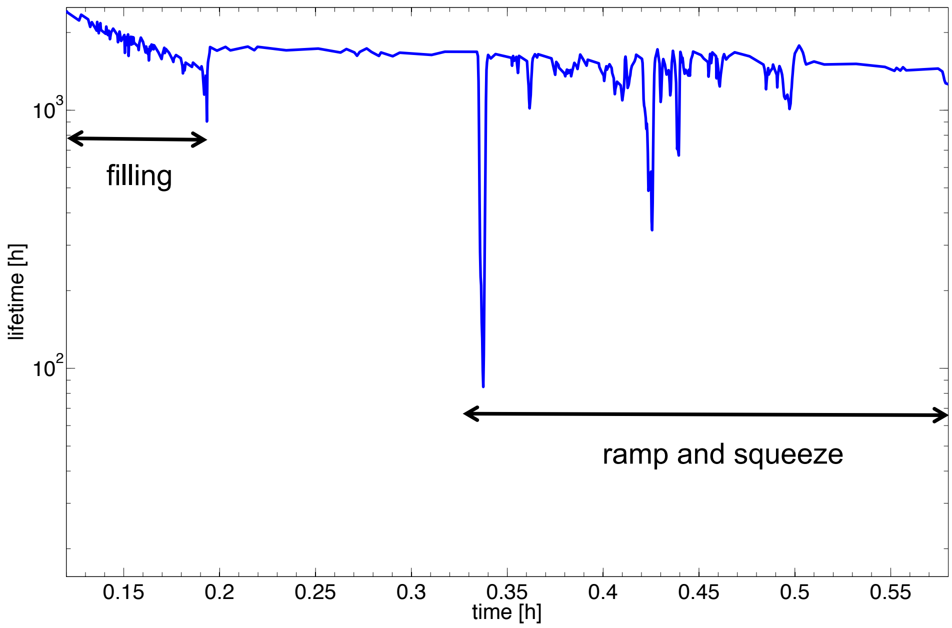

Fig. 9.6: Beam lifetime during injection, ramp and squeeze. One can see the lifetime dips during the ramp.

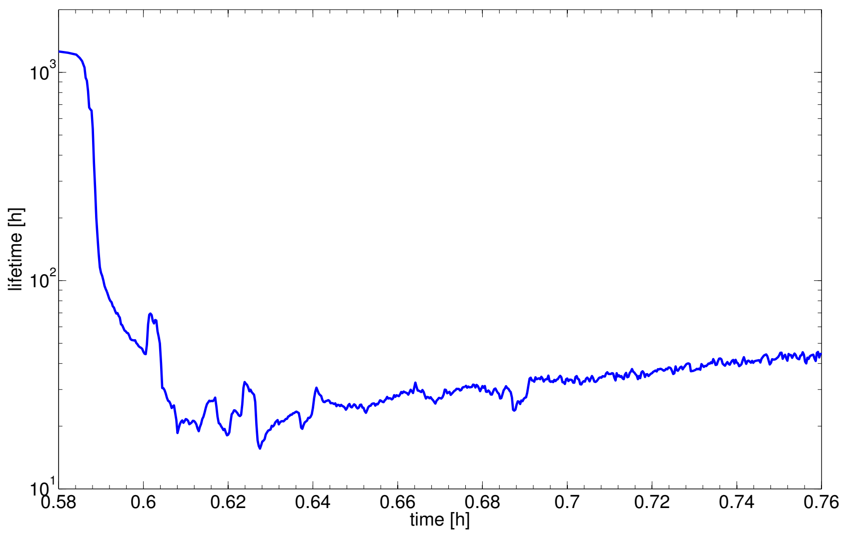

Fig. 9.7: Beam lifetime when the beams go into collision. One can see a dip in the lifetime down to 14.8 hours

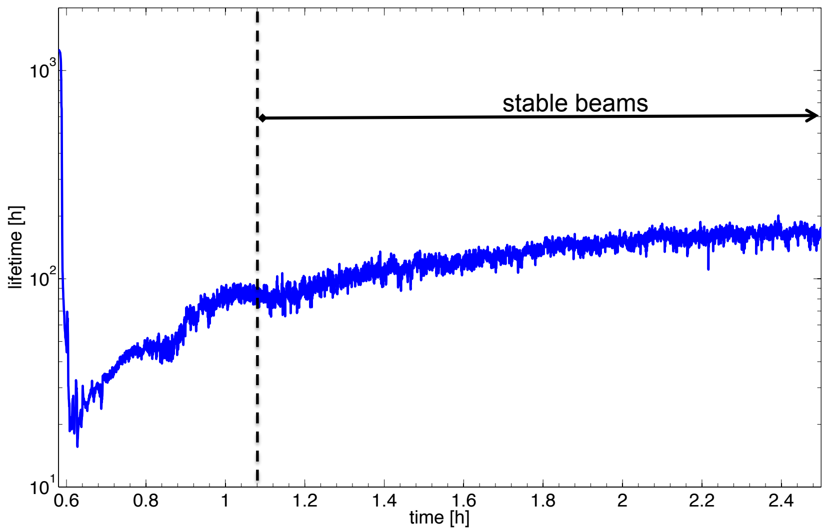

Fig. 9.8: Beam lifetime when going into collision and afterwards stable physics operation. The dip and the recovery of the lifetime after declaring stable beams back to an average value of 100 hours can be seen.

Tab. 9.2: Minimum lifetimes for both beams (RS09), the overall average of the lifetime, the averages for different values of β^* and after a tune change.

RS09	Beam 1	Beam 2
min. lifetime [h]	1.3	0.52
max. min. lifetime [h]	56	62
overall average [h]	9.9	16.8
with $\beta^* = 1.5$ m [h]	9.6	16.9
after tune change [h]	9.9	21.5
with $\beta^* = 1.0$ m [h]	10.0	13.4

Tab. 9.3: Minimum lifetimes for both beams (RS06), the overall average of the lifetime, the averages for different values of β^* and after a tune change is shown.

RS06	Beam 1	Beam 2
min. lifetime [h]	0.7	0.46
max. min. lifetime [h]	34	33
overall average [h]	5.6	6.9
with $\beta^* = 1.5$ m [h]	4.5	4.3
after tune change [h]	5.4	9.9
with $\beta^* = 1.0$ m [h]	7.6	9.5

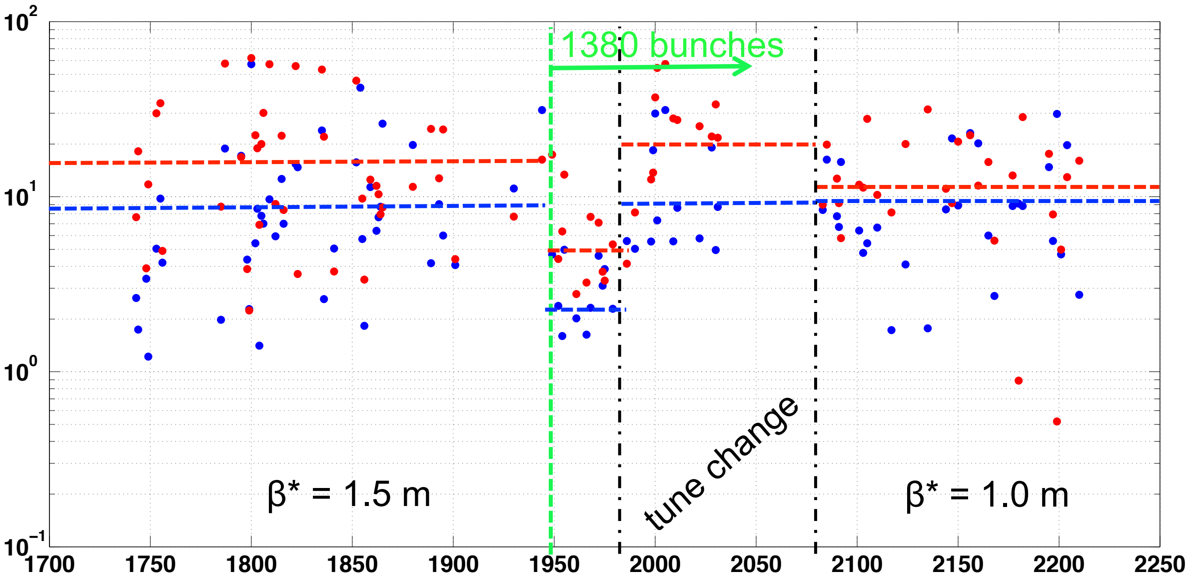

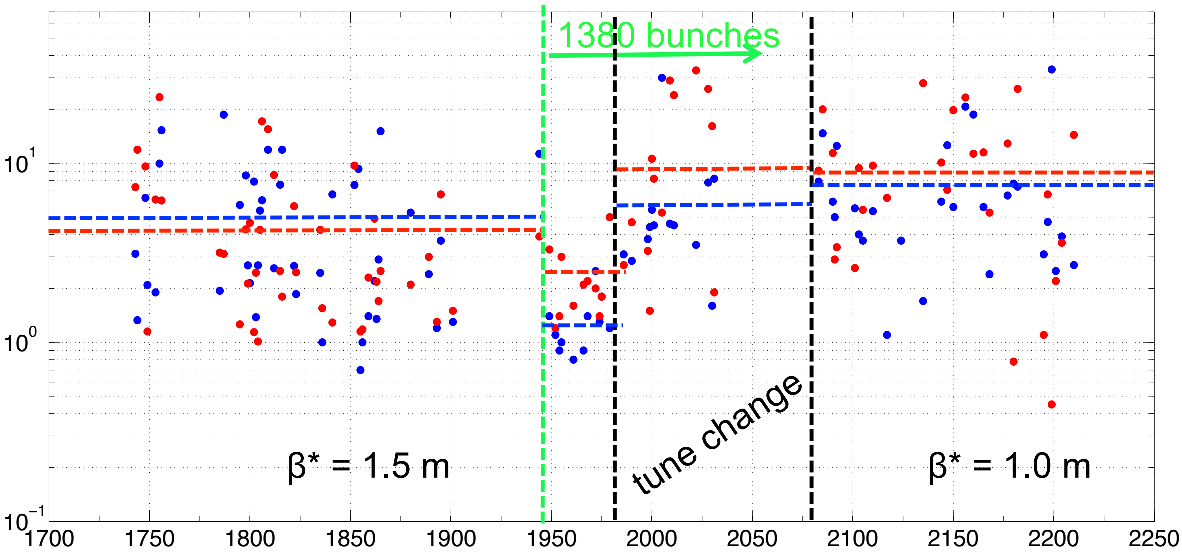

Fig. 9.9: **Top**: Minimum beam lifetime for beam modes adjust and stable beams for the running sum of 1.3 s. One can find a minimum beam lifetime of 0.55 h in Beam 2. Average minimum lifetimes are 9.8 h for Beam 1 and 17 h for Beam 2. **Bottom**: Minimum beam lifetimes for beam modes adjust and stable beams and the running sum of 10.24 ms. One can find a minimum beam lifetime of 0.45 h in Beam 2. Average minimum lifetimes are 5.6 h for Beam 1 and 6.9 h for Beam 2. Beam 1 is marked in blue, Beam 2 is marked in red. The minimum beam lifetime is plotted versus the fill number.

Tab. 9.4: Average lifetimes for both beams (RS09 and RS06), taking the best 90 % of the analysed fills.

	Beam 1	Beam 2
RS09 average lifetime [h]	11.1	18.9
RS06 average lifetime [h]	6.5	8.1
RS09 min. lifetime [h]	2.3	3.8
RS06 min. lifetime [h]	1.4	1.6

The minimum lifetime evaluated for the running sums RS02, RS04, RS06 and RS09 are depicted in Figure 9.12. A decrease of minimum beam lifetimes for smaller running sums was found.

Figure 9.10 and Figure 9.11 show a histogram of the minimum beam lifetimes for RS09 and RS06 for both beams and the 95 analysed physics fills in 2011.

A decrease of minimum beam lifetimes for smaller running sums was found. For RS06 27 of 95 fills (Beam 1) (22 for Beam 2) had a lifetime under 2 h. For RS09 10 of 95 fills (Beam 1) (3 for Beam 2) had a lifetime under 2 h. This analysis shows the dependence of machine behaviour on changes in the intensity, β^* and tune changes.

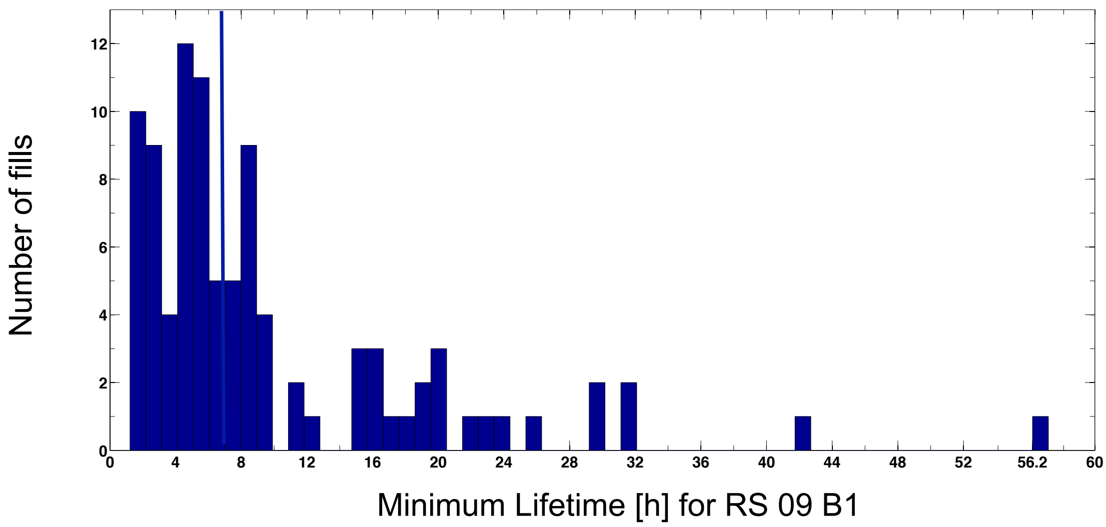

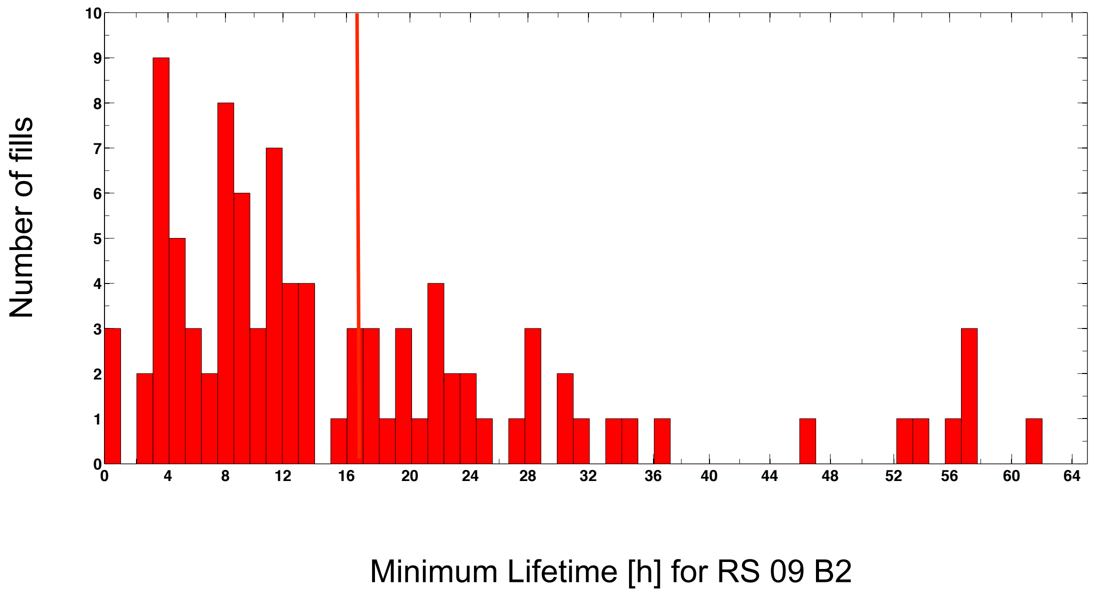

Fig. 9.10: Histogram of the minimum lifetimes for the running sum of 1.3 seconds for Beam 1 (blue) and Beam 2 (red). The averages of 9.8 h (B1) and 17 h (B2) are shown.

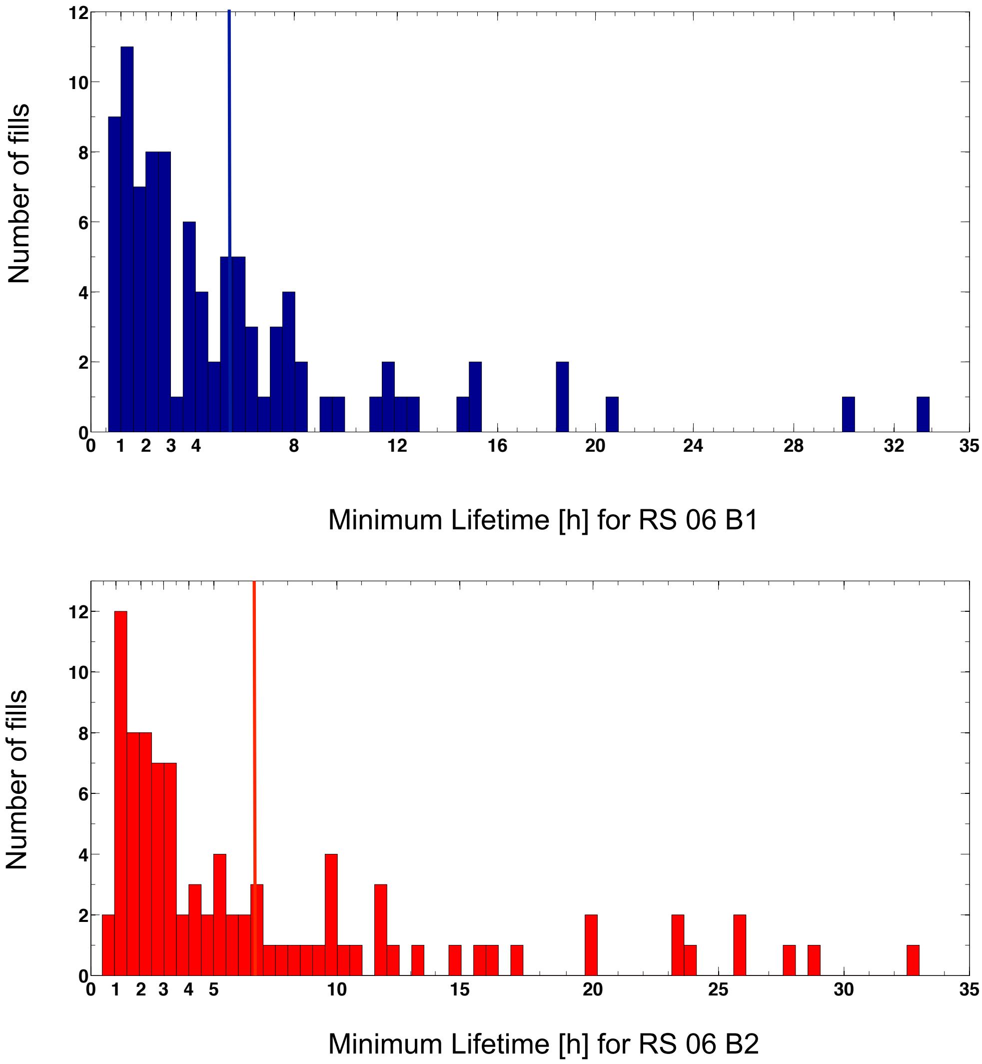

Fig. 9.11: Histogram of the minimum lifetimes for the running sum of 10.24 ms for Beam 1 (blue) and Beam 2 (red). The averages of 5.6 h (B1) and 6.9 h (B2) are shown.

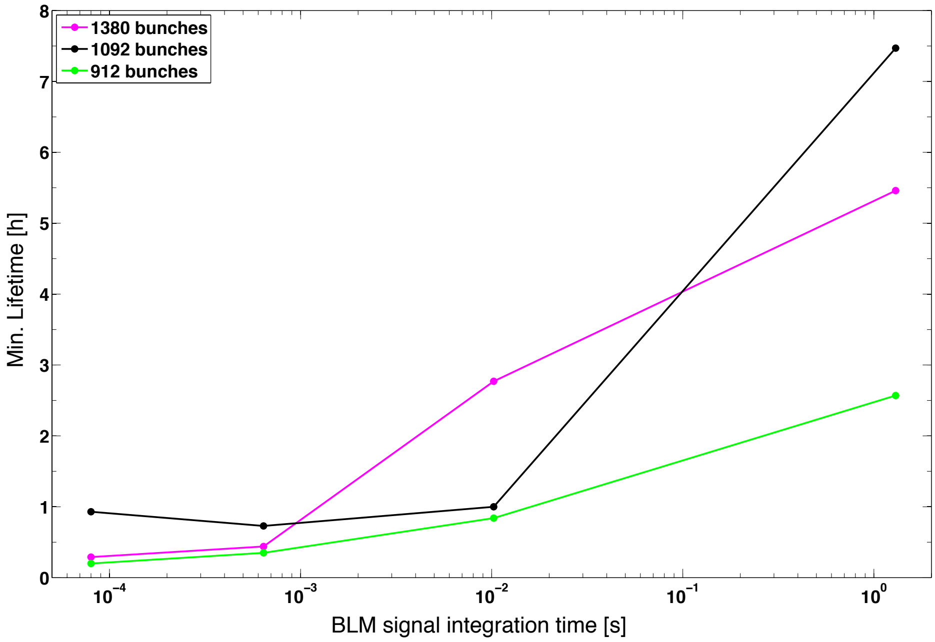

Fig. 9.12: Overview of the minimum values of the beam lifetime for one running sum. Going down in the running sum shows a decrease of the minimum beam lifetime.

10. CONCLUSION AND OUTLOOK

In this master thesis the beam loss and the beam shape at the LHC collimators was analysed, presented and discussed. A quantitative analysis of the beam loss at the collimators and at other locations around the ring was performed. With intensity measurements the BLM signals could be converted to a beam loss rate in p/s. This was used to demonstrate the design loss rate of 500 kW on a LHC primary collimator [32].

The lifetime during the 2011 proton physics fills in the LHC was analysed. This was done for different machine modes and for up to 110 MJ stored energy in one beam ($\sim$ 50 times previous world record). The results show that for losses at the collimators more than 11 h of minimum instantaneous lifetime can be maintained ($\sim$ 30 times better than specified) [34]. For the worst cases with a minimum instantaneous lifetime of 2.3 h this is still a factor 10 better than specified. The analysis of the lifetimes in the LHC also gives an insight into the impact of tune working point, changes in β^*, intensity increase, etc. The goal is to always reach low losses. Based on the presented results for the loss rates and for the lifetime at the collimators, the collimation upgrade plans were delayed by $\sim$ 5 years.

With beam halo scrapings the beam shape at the LHC primary collimators was measured. The results show over-populated tails, where up to $\sim$ 3 % of the particles are above 4 σ. This has an impact on machine protection and failure cases. The results of the beam shape measurements are now used as input for further studies by various colleagues.

Overall this master thesis shows the excellent performance of the LHC and its collimation system in 2011, supporting stable and successful physics operation. The results also show that at the moment there is no limitation from collimation for the performance reach of the LHC, even at a supposed beam energy of 7 TeV.

Future work should include the luminosity burn off at the experimental IRs and the losses in other regions of the LHC in the evaluation of the calibration factor. A more precise and optimistic value can then be obtained.

In the analysis of scraping the beam loss temporal tails are not fully understood yet. This is currently under investigation. Machine Development Time in 2012 will give additional data. In future work, the measured data for horizontal, vertical and skew scrapings could be combined to a two dimensional analysis of the transversal particle density in the LHC beams.

11. ZUSAMMENFASSUNG

Der **L**arge **H**adron **C**ollider (LHC) bringt zwei gegenläufige Protonen- oder Bleiionenstrahlen an vier Wechselwirkungspunkten (IPs) zur Kollision. In den IPs sind die Detektoren der vier Hauptexperimente des LHC installiert. Sie heißen ATLAS, ALICE, CMS und LHCb. 2011 wurden in ATLAS und CMS bis zu 5.6 fb^{-1} an integrierter Luminosität erreicht. Dies entspricht mehr als der Hälfte der integrierten Luminosität die das Tevatron innerhalb seiner Betriebsdauer gemessen hat. Um dies zu erreichen werden hohe Strahlintensitäten im LHC benötigt. Im Jahr 2011 wurde eine maximale Intensität von $\sim 2 \times 10^{14}$ (Designwert: $\sim 3.2 \times 10^{14}$) Protonen pro Strahl gespeichert. Bei einem Teilchenimpuls von 3.5 TeV/c entspricht dies einer gespeicherten Energie von 116 MJ pro Strahl (Designwert bei 7 TeV/c: 362 MJ).

Um Teilchenstrahlen mit solch einem hohen Impuls zu speichern werden supraleitende Magnete benötigt. Das Limit bei der solch ein Magnete seine supraleitenden Eigenschaften verliert (Quench) liegt bei $\sim 7.6 \times 10^6$ Protonen pro Sekunde und Meter, das entspricht ungefähr 5-40 mJ/cm^3. Verglichen mit der gespeicherter Intensität heißt dies, dass im LHC Verluste im Promillebereich einen Quench induzieren würden. Teilchenverluste sind jedoch aufgrund von Streuung am Restgas, Strahl-Strahl-Wechselwirkung, etc. unvermeidbar.

Um einen unkontrollierten Verlust dieser gestreuten Teilchen im LHC-Ring zu vermeiden müssen diese durch Kollimatoren aufgefangen werden. Die Kollimatoren stellen dabei die kleinste Öffnung der Apertur im LHC dar. Zusätzlich übernehmen die Kollimatoren im Fall eines Fehlers, der zu hohen Strahlverlusten führt, eine passive Schutzfunktion. Im LHC ist ein 4-stufiges Kollimationssystems installiert, dessen Performance regelmäßig mit sogenannten Lossmaps geprüft wird (siehe Abbildung 6.1). Dabei werden die Teilchenverluste mit Ionisationskammern, den sogenannten Beam Loss Monitoren, die um den ganzen Ring installiert sind, in Gy/s gemessen.

Die Masterarbeit mit dem Titel *Beam Loss and Beam Shape at the LHC collimators* wurde zwischen März 2011 und März 2012 in der LHC-Kollimations-Arbeitsgruppe des CERN geschrieben. Betreut wurde diese Arbeit von Dr. Ralph W. Aßmann (Projektleiter LHC Kollimation, CERN) und Prof. Dr. Ulrich Ratzinger (Institut für Angewandte Physik, Goethe-Universität Frankfurt/ Main).

In dieser Masterarbeit wurden die beobachteten Verluste mithilfe von berechneten Kalibrationsfaktoren in Teilchenverlustraten (p/s) umgerechnet. Die dadurch erhaltenen Verlustraten konnten dann in eine Verlustleistung umgerechnet werden. Abbildung 11.1 zeigt die Verlustleistung um den gesamten LHC-Ring während eines Experiments in Strahl 2.

Bei einer Teilchenverlustrate von 9×10^{11} p/s wurde eine maximale Verlustleistung von 505 kW am primären Kollimator in IR7 für die Dauer einer Sekunde erreicht. Die höchste Verlustleistung an einem supraleitenden Magneten lag bei 335 W und wurde im sogenannten Q8 links von IR7 gemessen. In diesem Experiment wurde die für 7 TeV spezifizierte maximale Verlustleistung an einem primären Kollimator erreicht ohne dabei einen Quench zu verursachen.

Die maximal im LHC erreichbare Strahlintensität ist u.a. durch die Performance des Kollimationssystems limitiert:

$$N_{max} \sim \tau \cdot R_{max}. \tag{11.1}$$

Hierbei ist R_{max} die maximale gemessene Verlustrate an einem primären Kollimator ohne dass ein Magnet quencht und τ die minimale Lebensdauer die durch Verluste am Kollimationssystem bestimmt ist.

Die minimale Kollimationsabhängige Lebensdauer kann aus den BLM-Daten mithilfe des oben erwähnten Kalibrationsfaktors direkt bestimmt werden (siehe Gleichung 9.1). Während dieser Masterarbeit wurden alle Protonen-Physik-Füllungen des Jahres 2011 bezüglich ihrer minimalen Lebensdauer analysiert. Die minimale Lebensdauer pro Füllung ist in Abbildung 11.2 dargestellt. Die mittlere minimalen Lebensdauer betrug dabei 11 h (19 h) für Strahl 1 (Strahl 2). Mithilfe dieser Analyse wurde das kollimationsinduzierte Intensitätslimit des LHC bei einem Teilchenimpuls von 3.5 TeV/c auf 1.0×10^{16} Protonen abgeschätzt. Dies entspricht dem 30-fachen nominellen Wert [34]. Deshalb wurden die Upgrade-Pläne für das LHC-Kollimationssystem um circa 5 Jahre verschoben.

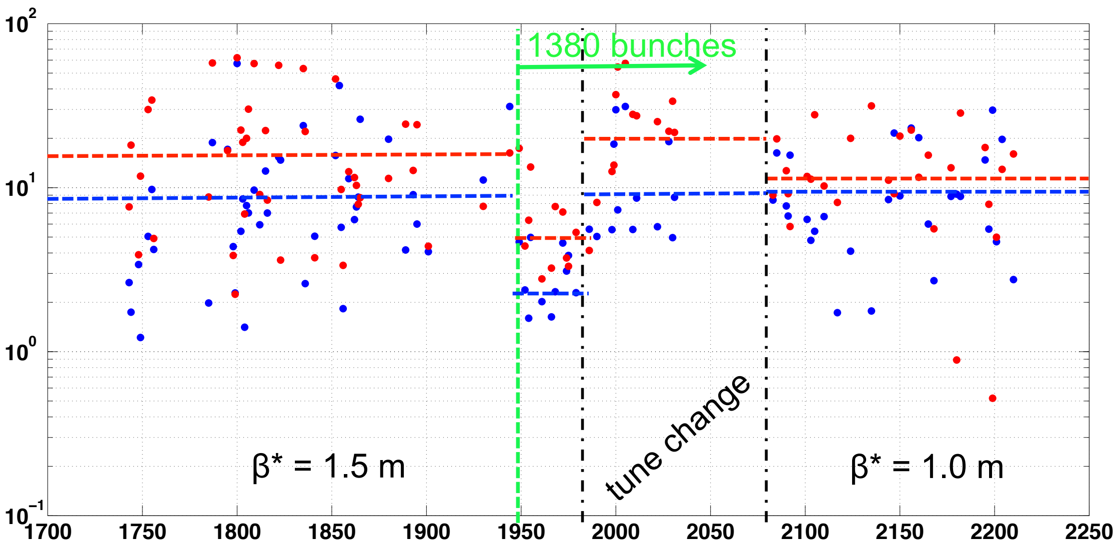

Fig. 11.2: Minimale Lebensdauern für den Modus *adjust* und *stable beams*. Strahl 1 ist in blau, Strahl 2 in rot dargestellt.

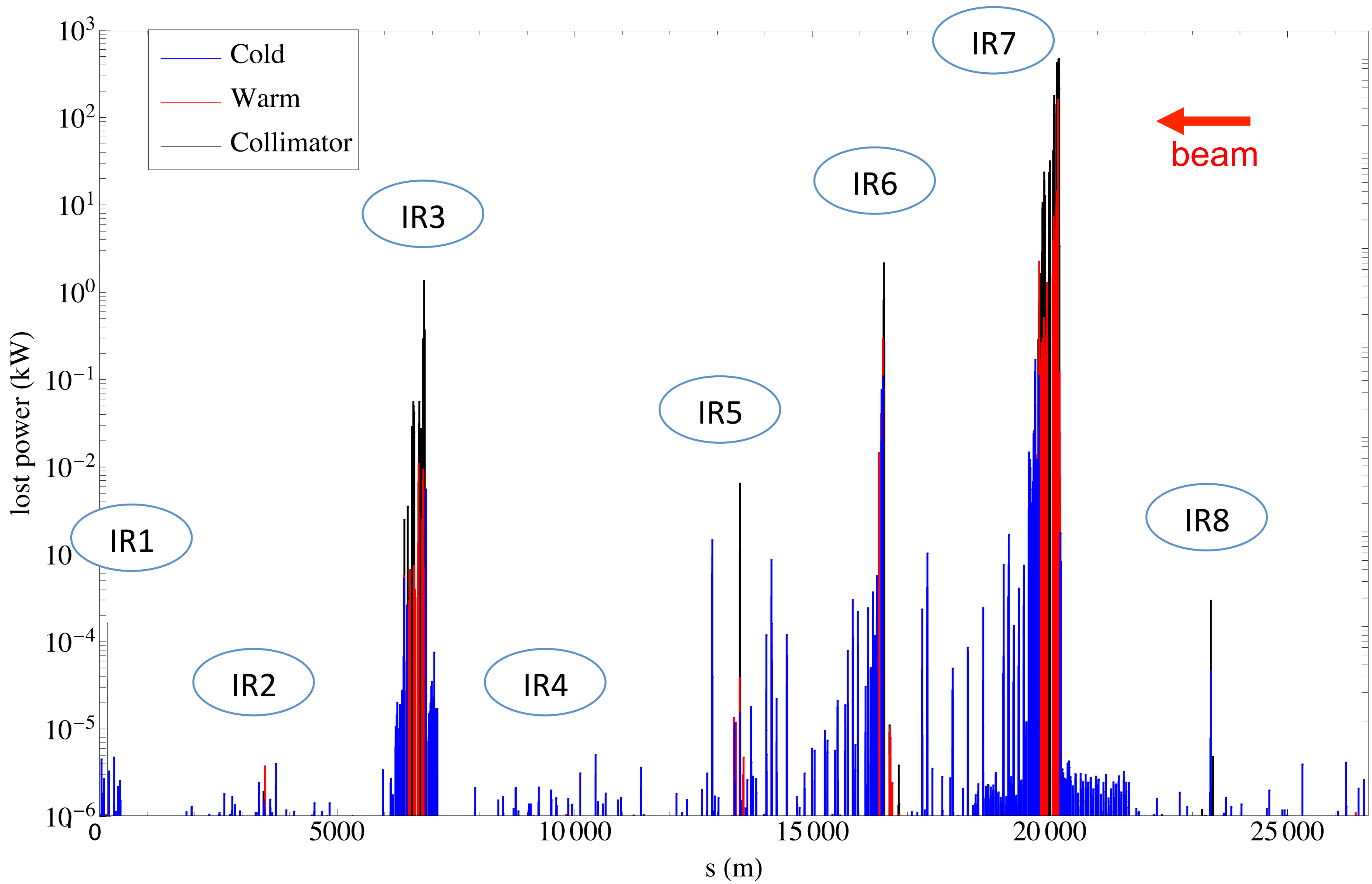

Fig. 11.1: Lossmap in Strahl 2. Die maximale Verlustleistung von 505 kW trat am primären Kollimator in IR7 auf. Die höchste Verlustleistung wurde im sogenannten Q8 links von IR7 gemessen.

In Abbildung 11.2 kann man erkennen, dass die minimale Lebensdauer von Änderungen der Maschinenparameter abhängt. Dies ist in Kapitel 9 beschrieben.

In dieser Arbeit wurde zum ersten Mal die transversale Teilchenverteilung in verschiedenen Strahlebenen (horizontal, vertikal und skew) mithilfe der primären Kollimatoren gemessen. Diese sogenannten *Halo-scrapings* wurde sowohl bei Injektionsenergie (450 GeV) als auch bei 3.5 TeV durchgeführt.

Abbildung 11.3 zeigt die gemessene transversale Strahlverteilung bei 450 GeV in horizontaler, vertikaler und skew Ebene, in Abbildung 11.4 wird die gemessene Strahlverteilung bei 450 GeV (blau) und 3.5 TeV (rot) verglichen. Man kann erkennen, dass die gemessene Verteilung in den Tails deutlich von einer gauss-förmigen Verteilung abweicht.

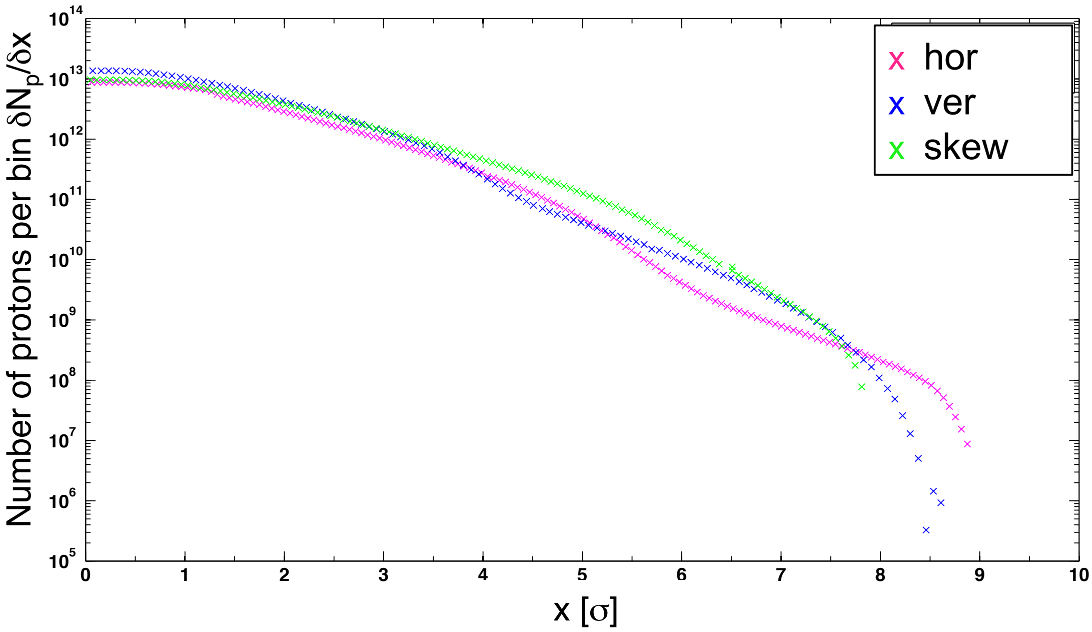

Fig. 11.3: Transversale Teilchenverteilung im LHC in verschiedenen Strahlebenen. Horizontal (rot), vertikal (blau), skew (grün). Diese Halo-scrapings wurden alle mit einer Schrittweite von 20 μm und bei 450 GeV durchgeführt.

Es wurden bis zu 3.6 % der Teilchen ausserhalb von 4σ gefunden. Skaliert zu Designintensität und Designenergie sind bis zu 16 MJ in den Tails gespeichert. Die Abweichung von einer gauss-förmige Strahlverteilung, wie man sie zum Beispiel in Elektronenmaschinen misst, kann, im Fall von Protonen, durch die vielfach geringere Synchrotronstrahlungsdämpfung erklärt werden.

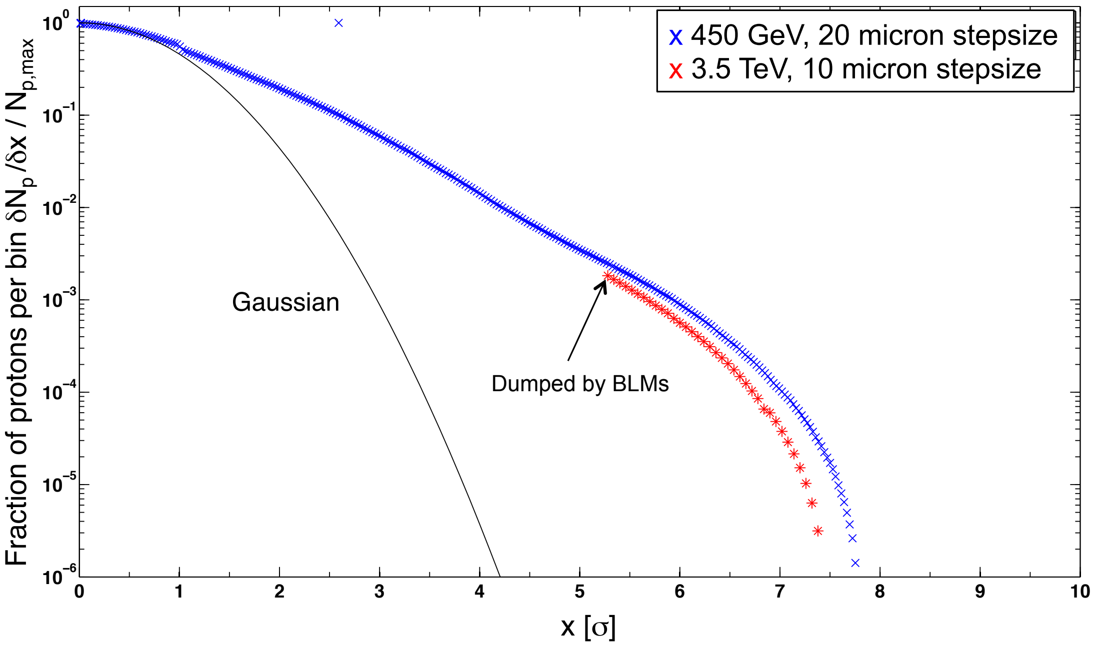

Fig. 11.4: Vergleich der transversalen Teilchenverteilung in der horizontalen Ebene bei 450 GeV (blau) und 3.5 TeV (rot). Zum Vergleich wurde eine Gauss-Kurve (schwarz) eingezeichnet.

Die in dieser Masterarbeit gemessenen transversalen Strahlverteilungen sind eine wichtige Grundlage für weiterführende Studien über zukünftige LHC-Upgrades.

12. ACKNOWLEDGEMENTS

The author wants to thank Dr. Ralph W. Assmann from the BE-ABP department at CERN for giving him the possibility to write this master thesis at CERN, his support, his critical comments, discussions and scientific supervision throughout the whole period this thesis has been elaborated.
The author also wants to thank Prof. Dr. Ulrich Ratzinger from the institute for applied physics (IAP) at the Goethe-University Frankfurt for giving him the possibility to write this master thesis, his support, critical comments and scientific supervision.
The author especially wants to thank Dr. Daniel Wollmann (CERN) for a lot of day-to-day support, all the discussions, critical comments, his scientific supervision and his friendship.
The work was performed with the help of the whole collimation working group. The author wants to thank Dr. R. Bruce, M. Cauchi, D. Deboy, S. Hillenbrand, Dr. S. Redaelli, Dr. A. Rossi, Dr. B. Salvachua-Ferrando and G.Valentino for their help during measurements, their helpful discussions and support.
The author wants to thank his parents for giving the possibility to study physics and their support.
Finally the author wants to thank Sonja Bühler for her great support and patience.

BIBLIOGRAPHY

[1] CERN press office. LHC facts. http://press.web.cern.ch/public/en/LHC/Facts-en.html, 2011.

[2] LHC Design report. Volume 1 - The main ring. Editorial board, CERN, 2004.

[3] LHC Design report. Volume 1 - Layout and Performance. Editorial board, CERN, 2004.

[4] ATLAS Collaboration. http: //atlas.web.cern.ch

[5] CMS Collaboration. http: //cmsinfo.cern.ch

[6] ALICE Collaboration. http: //aliceinfo.cern.ch

[7] LHCb Collaboration. http: //lhcb.web.cern.ch

[8] LHC-statistics. LHC OP team. http: //lhc-statistics.web.cern.ch/LHC-Statistics. 2011.

[9] LHC Design report. Volume 1 - Beam Parameters and Definitions. Editorial board, CERN, 2004.

[10] LHC Design report. Volume 1 - Main magnets in the arcs. Editorial board, CERN, 2004.

[11] R.W. Assmann. Beam commissioning of the collimation system. In proceedings of Chamonix XV, CERN.

[12] R. Schmidt, TE-MPE-PE, CERN, Geneva, Switzerland

[13] C. Bracco. Commissioning Scenarios and Tests for the LHC Collimation System. PhD thesis, Ecole Polytechnique Federale de Lausanne and CERN. 2008.

[14] R.W. Assmann et al. Requirements for the LHC Collimation System. In Proceedings of the European Particle Accelerator Conference, EPAC, Paris, France. 2002.

[15] LHC Design report. Volume 1 - The RF-System and beam feedback. Editorial board, CERN, 2004.

[16] R. Schmidt. LHC Machine Protection. In proceedings of 22nd Particle Accelerator Conference, PAC, Albuquerque, USA. 2007.

[17] LHC Design report. Volume 1 - Beam Instrumentation. Editorial board, CERN, 2004.

[18] B. Dehning. Beam loss monitor system overview and reliability. 2008

[19] K. Wille. Physik der Teilchenbeschleuniger und Synchrotronstrahlungsquellen, chapter 3: Lineare Strahloptik. 1996

[20] R.W. Assmann. The phased implementations of LHC Collimation. In proceedings of HHH. 2008

[21] G. Robert-Demolaize. Design and Performance Optimizations of the LHC Collimation System. PhD thesis, Universite Joseph Fourier, Grenoble. 2006.

[22] D. Wollmann. First cleaning with LHC Collimators. In proceedings of IPAC10, Kyoto, Japan. 2010.

[23] R.W. Assmann, BE-ABP-LCU, CERN, Geneva, Switzerland

[24] R.W. Assmann et al. Collimators and Beam Absorbers for Cleaning and Machine Protection. In LHC Project Workshop-Chamonix XIV, 2005.

[25] A. Bertarelli et al. The mechanical design for LHC Collimators. In proceedings of the European Particle Accelerator Conference, EPAC04, Lucerne, Switzerland. 2004

[26] R.W. Assmann. Summary of the collimation upgrade plans. In proceedings of EuCard. 2010.

[27] CERN-LARP collaboration webpage. LARP-Meetings: The secondary collimator project.

[28] G. Stancari. Development of hollow electron beams for proton and ion collimation. FERMILAB-CONF-10-182-AD-APC.

[29] D. Wollmann et al. Multiturn losses and cleaning. 2010.

[30] D. Wollmann et al. Collimation dependent beam lifetime and loss rates in the LHC. In proceedings of IPAC11, San Sebastian, Spain. 2011.

[31] R.W. Assmann. The final LHC Collimation System.

[32] R.W. Assmann et al. Collimation losses in the DS of IR7 and quench test at 3.5 TeV. CERN-ATS-Note-2011-042 MD (LHC). 2011.

[33] R.W. Assmann et al. Beam distribution measurements in the LHC. CERN-ATS-Note-2011-057 MD (LHC). 2011.

[34] R.W. Assmann. LHC Collimation Review. CERN. June 2011.